Dispersion phenomena of reactive solute in a pulsatile flow of three-layer liquids

Sudip Debnath, Apu Kumar Saha, B. S. Mazumder, and Ashis Kumar Roy

Citation: Physics of Fluids **29**, 097107 (2017); doi: 10.1063/1.5001962
View online: http://dx.doi.org/10.1063/1.5001962
View Table of Contents: http://aip.scitation.org/toc/phf/29/9
Published by the American Institute of Physics

Dispersion phenomena of reactive solute in a pulsatile flow of three-layer liquids

Sudip Debnath,[1,a)] Apu Kumar Saha,[1,b)] B. S. Mazumder,[2,c)] and Ashis Kumar Roy[1,d)]
[1]*Department of Mathematics, National Institute of Technology, Agartala 799046, India*
[2]*Fluvial Mechanics Laboratory, Physics and Applied Mathematics Unit, Indian Statistical Institute, Kolkata 700108, India*

(Received 20 March 2017; accepted 26 August 2017; published online 28 September 2017)

This study aims at investigating the dispersion process in an oscillatory flow of a layered liquid. The liquid is considered as a three-layer liquid where the center region is the Casson liquid surrounded by a Newtonian liquid layer flowing through a narrow pipe under the wall reaction. The perturbation technique has been used for solving the momentum equations. In order to assist the analysis of solute transport behavior, Aris-Barton's method of moments has been utilized, where different molecular diffusivities were assumed for different respective regions, yet to be constant. The effects of finite yield stress, viscosity ratio, density ratio, peripheral layer thickness, and irreversible absorption at the tube wall on dispersion are investigated in detail. In the cases of steady, unsteady, and combined flow situations, dispersion coefficient is found to be diminished by absorption parameter, viscosity ratio, and yield stress, respectively. In the case of a steady flow and unsteady convective diffusion of a reactive solute, dispersion coefficient is independent of density ratio. For both the unsteady and combined flows, density ratio provides a pulsatile behaviour of the dispersion process though an increase in the density ratio may faster the dispersion process. Dispersion at early times is not affected by absorption though a considerable effect is observed for large time. The presence of a peripheral layer enhances the value of the dispersion coefficient and is higher than the single layer Casson liquid flow. As strong as the non-Newtonian effect is considered, the dispersion process becomes slower. Larger values of molecular diffusivity at different layers are the reason for less dispersion coefficient. This study may be useful for understanding the dispersion process in the blood-like liquid flow analysis for microcirculation. *Published by AIP Publishing.* https://doi.org/10.1063/1.5001962

I. INTRODUCTION

In a solute transport process, dispersion is one of the mechanisms which is utilized as an efficient means to accomplish dilution or mixing. Due to its wide applications in the field of chemical engineering, physiological fluid dynamics, environmental sciences, biomedical engineering, etc., it has been extensively studied for the past six decades. Transport under the effects of wall reactions has long been drawing attention as it is important to many industrial and physiological situations, e.g., chromatography, absorption of gases in airways, electrophoresis, human arteries, flow through fractures, etc. The classical work of dispersion has been started by Taylor,[47] theoretically and experimentally. Aris[5] extended Taylor's theory and developed an approach called "method of moments" to analyze the asymptotic behaviour of second order moment about the mean. These two models apply only at long times. Gill and Sankarasubramanian[20] and Barton[8] used elegant all-time approaches to study the dispersion of passive solutes in Newtonian fluid flows. A numerical study was performed by Ananthakrishnan *et al.*[3] to solve the convective diffusion equation by the standard finite difference method and showed that the Taylor-Aris dispersion theory can be applied only for a sufficiently large value of the dimensionless time.

Mathematical studies on solute dispersion have largely been discussed in both the Newtonian[23–25,27,33,34] and non-Newtonian[1,35–37,44,46] environments, subject to steady and unsteady flows through a straight and curved tube or channel or annulus with or without chemical reactions. There are published studies[7,26,31,42] in the literature dealing with the application of dispersion to a catheterized artery. In modern days, dispersion in non-Newtonian fluids is being widely followed for various applications. The assumption of a passive solute and the Newtonian description for the solvent may be too restrictive. Studies on the Casson fluid with respect to low yield stress can be well appreciated[10,13,28] to characterize the blood flow analysis under the consideration of haematocrits, anticoagulants, temperature, etc. In blood flow, the yield stress considerably affects the rate of dispersion of the fluid.[17] When the blood flows through small blood vessels, the presence of a peripheral layer of plasma (Newtonian liquid) and a core region of suspension of all the erythrocytes as a non-Newtonian liquid has been found, which was experimentally shown by

[a)]Electronic mail: sudipdebnath49@gmail.com
[b)]Author to whom correspondence should be addressed: apusaha_nita@yahoo.co.in
[c)]Present address: Fluid Mechanics and Hydraulic Laboratory (FMHL), Department of Aerospace Engineering and Applied Mechanics, Indian Institute of Engineering Science and Technology (IIEST), Shibpur, Howrah 711 103, India. Electronic mail: bsmazumder@gmail.com
[d)]Electronic mail: rk.ashis10@gmail.com

Bugliarello and Sevilla[11] and Cokelet.[14] Thus, for a practical portrayal of the blood stream, it is more appropriate to regard the blood as a two-liquid (or three-layer liquid) model comprising all the erythrocytes thought to be the Casson liquid and a peripheral layer of plasma as a Newtonian liquid. In the recent work of Debnath *et al.*[18] and Rana and Murthy,[38] the dispersion process through a three-layer liquid continuum has been studied under the steady and unsteady nature of liquid spreading. The present study considers the following features:

(1) a three-layer liquid of a Casson-Newtonian continuum has been considered, (2) the periodic pressure gradient is the reason of flow pulsation, (3) the solute is supposed to undergo a first-order reaction (irreversible absorption) into the boundary of a pipe, (4) in contrast to the published studies in this direction, the present study has investigated the parametric effect of molecular diffusivity at different liquid layers which has helped one to project the importance of viscosity ratio and density ratio in hydrodynamic dispersion.

In a layered liquid flow, density and viscosity ratios are responsible for the dynamics of the interaction.[9,21,39] These studies suggest that effects of viscosity and density ratios are more significant than those of the previously recognized works in the computational and experimental studies of a multiphase flow. The plug flow within the Casson region is very important because the significant advantage of transporting particulate materials in a plug form is of low energy consumption, low particles attrition, and low pipe erosion.[45] The main objective of the present study is to understand the physical mechanism of contaminant mixing and to provide a theoretical framework to interpret the spreading of a contaminant in a pulsatile blood-like liquid flow with an irreversible wall reaction.

II. MATHEMATICAL FORMULATION

A uni-directional, unsteady laminar, axi-symmetric, fully developed flow of an incompressible, three-layer liquid through a circular pipe of radius $\overline{R}$ is considered (Fig. 1). The core region of radius $\overline{R}_o$ ($\leq\overline{R}$) is supposed to be a non-Newtonian liquid surrounded by the Newtonian liquid layer. A cylindrical coordinate system is considered where the axial and radial coordinates are represented by $\overline{z}$ and $\overline{r}$, the over bar represents the dimensional quantities. The non-Newtonian behaviour of the liquid is described by the Casson liquid in Ref. 6. On account of enough axial covering of the tube, and for low Reynolds number flow, it can be shown that the radial velocity is negligibly small and can be disregarded,

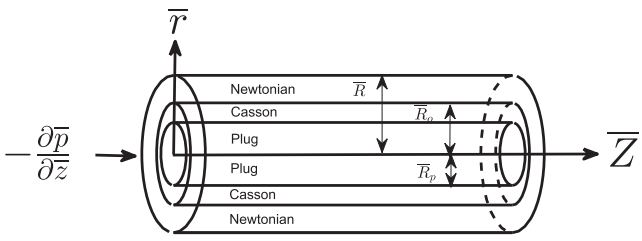

FIG. 1. Schematic diagram of the setup under consideration.

TABLE I. Liquid properties assigned for Casson and Newtonian liquids.

Physical quantity	Symbol for Casson liquid	Symbol for Newtonian liquid
Density	$\overline{\rho}_c$	$\overline{\rho}_n$
Shear stress	$\overline{\tau}_c$	$\overline{\tau}_n$
Velocity	$\overline{u}_c$	$\overline{u}_n$
Viscosity	$\overline{\mu}_c$	$\overline{\mu}_n$

thus a fully developed flow is considered only in the axial direction. The pressure gradient at any $\overline{z}$ is given by

$$-\frac{\partial\overline{p}}{\partial\overline{z}} = A_0 + A_1\sin(\omega_p\overline{t}), \tag{1}$$

where A_0 is a steady component of pressure gradient, A_1 is an amplitude of fluctuating component, $\omega_p = 2\pi f_p$, where f_p is the pulse frequency, $\overline{t}$ is the time, and $\overline{p}$ is the pressure.

The governing equations of motion for the flow in axial direction are given by

$$\overline{\rho}_c\frac{\partial\overline{u}_c}{\partial\overline{t}} = -\frac{\partial\overline{p}}{\partial\overline{z}} - \frac{1}{\overline{r}}\frac{\partial(\overline{r}\,\overline{\tau}_c)}{\partial\overline{r}}, \quad 0\leq\overline{r}\leq\overline{R}_o, \tag{2}$$

$$\overline{\rho}_n\frac{\partial\overline{u}_n}{\partial\overline{t}} = -\frac{\partial\overline{p}}{\partial\overline{z}} - \frac{1}{\overline{r}}\frac{\partial(\overline{r}\,\overline{\tau}_n)}{\partial\overline{r}}, \quad \overline{R}_o\leq\overline{r}\leq\overline{R}. \tag{3}$$

The relation between shear stress and strain rate in the Casson region $\mathcal{R}_c$ (=$[0,\overline{R}_o]$) and Newtonian region $\mathcal{R}_n$ (=$[\overline{R}_o,\overline{R}]$) is given by the following constitutive relations:

$$\left.\begin{array}{lll} \overline{\tau}_c^{\frac{1}{2}} = \overline{\tau}_y^{\frac{1}{2}} + (-\overline{\mu}_c\frac{\partial\overline{u}_c}{\partial\overline{r}})^{\frac{1}{2}} & \text{if} & \overline{\tau}_c\geq\overline{\tau}_y \text{ for } \overline{R}_p\leq\overline{r}\leq\overline{R}_o \\ \frac{\partial\overline{u}_c}{\partial\overline{r}} = 0 & \text{if} & \overline{\tau}_c\leq\overline{\tau}_y \text{ for } 0\leq\overline{r}\leq\overline{R}_p \\ \overline{\tau}_n = -\overline{\mu}_n\frac{\partial\overline{u}_n}{\partial\overline{r}} & \text{if} & \overline{\tau}_y = 0 \text{ for } \overline{R}_o\leq\overline{r}\leq\overline{R} \end{array}\right\}, \tag{4}$$

with the boundary conditions

$$\left.\begin{array}{ll} \overline{\tau}_c \text{ is finite and } \frac{\partial\overline{u}_c}{\partial\overline{r}} = 0 & \text{at } \overline{r} = 0 \\ \overline{\tau}_c = \overline{\tau}_n \text{ and } \overline{u}_c = \overline{u}_n & \text{at } \overline{r} = \overline{R}_o \\ \overline{u}_n = 0 & \text{at } \overline{r} = \overline{R} \end{array}\right\}, \tag{5}$$

where $\overline{\tau}_y$ is the yield stress and $\overline{R}_p$ is the plug core radius. In relation (4), whenever $\overline{\tau}_c\leq\overline{\tau}_y$, the velocity gradient will be zero, as a consequence, a plug flow region will appear within the Casson region. Table I represents the liquid properties with their corresponding symbols.

III. CONVECTION-DIFFUSION EQUATION

Let us contemplate the transport and spreading of a chemical species with the fluid flowing through a tube which is supposed to be so dilute that the presence of the chemical species will not affect the carrier flow. The species involve in a kind of reaction (irreversible absorption) into the wall. The transport equation that governs the concentration $\overline{C}(\overline{t},\overline{r},\overline{z})$ is the unsteady convective diffusion equation and is given by

$$\frac{\partial\overline{C}}{\partial\overline{t}} + \overline{u}(\overline{r},\overline{t})\frac{\partial\overline{C}}{\partial\overline{z}} = \frac{\overline{D}}{\overline{r}}\frac{\partial}{\partial\overline{r}}\left(\overline{r}\frac{\partial\overline{C}}{\partial\overline{r}}\right) + \overline{D}\frac{\partial^2\overline{C}}{\partial\overline{z}^2}, \tag{6}$$

where $\overline{D}$ is the constant molecular diffusivity chosen to be different in the three regions $\mathcal{R}_p$, $\mathcal{R}_c$, and $\mathcal{R}_n$. So we assume

$$\overline{D} = \begin{Bmatrix} \overline{D}_p & \text{in } \mathcal{R}_p \\ \overline{D}_c & \text{in } \mathcal{R}_c \\ \overline{D}_n & \text{in } \mathcal{R}_n \end{Bmatrix}. \tag{7}$$

The initial and boundary conditions for the transport Eq. (6) are considered as

$$\left.\begin{aligned} \overline{C}(0,\overline{r},\overline{z}) &= \overline{C}_0 B(\overline{r})\psi(\overline{z}), \quad (0 < \overline{r} < \overline{R}) \\ C_0 &= \frac{M}{\pi \overline{R}^3} \\ \psi(\overline{z}) &= \overline{R}\,\delta(\overline{z}) \\ B(\overline{r}) &= 1 \end{aligned}\right\}, \tag{8}$$

$$\frac{\partial \overline{C}}{\partial \overline{r}} = 0 \quad \text{at} \quad \overline{r} = 0, \tag{9}$$

$$\frac{\partial \overline{C}}{\partial \overline{r}} + \overline{\beta}\,\overline{C} = 0 \quad \text{at} \quad \overline{r} = \overline{R}. \tag{10}$$

The initial solute distribution at $\overline{t} = 0$ is considered by introducing the solute of mass M, where $B(\overline{r})$ is a function of $\overline{r}$, and $\delta(\overline{z})$ is the Dirac delta function. The absorbing boundary condition at the wall of the tube is represented by Eq. (10) where $\overline{\beta}$ is the first-order reaction rate.

Using the following dimensionless quantities:

$$\left.\begin{aligned} &t = \frac{\overline{D}_n \overline{t}}{\overline{R}^2},\ r = \frac{\overline{r}}{\overline{R}},\ z = \frac{\overline{D}_n \overline{z}}{\overline{R}^2 u_0},\ u_0 = \frac{\overline{R}^2 A_0}{4\overline{\mu}_n}, \\ &u_c = \frac{\overline{u}_c}{u_0},\ u_n = \frac{\overline{u}_n}{u_0}, C = \frac{\overline{C}}{\overline{C}_0},\ \tau_c = \frac{\overline{\tau}_c}{\overline{\mu}_n(\frac{u_0}{\overline{R}})}, \\ &\tau_n = \frac{\overline{\tau}_n}{\overline{\mu}_n(\frac{u_0}{\overline{R}})},\ R_0 = \frac{\overline{R}_o}{\overline{R}},\ R_p = \frac{\overline{R}_p}{\overline{R}},\ \tau_y = \frac{\overline{\tau}_y}{\overline{\mu}_n(\frac{u_0}{\overline{R}})}, \\ &\beta = \overline{\beta}\,\overline{R},\ Pe = \frac{u_0 \overline{R}}{\overline{D}_n},\ m = \frac{\overline{\mu}_c}{\overline{\mu}_n},\ n = \frac{\overline{\rho}_c}{\overline{\rho}_n}, \\ &D^* = \frac{\overline{D}}{\overline{D}_n},\ Sc = \frac{\overline{\nu}_n}{\overline{D}_n},\ \alpha^2 = \frac{\overline{R}^2 \omega_p}{\overline{\nu}_n}, \end{aligned}\right\} \tag{11}$$

Eqs. (6)–(10) become

$$\frac{\partial C}{\partial t} + u(r,t)\frac{\partial C}{\partial z} = \frac{D^*}{r}\frac{\partial}{\partial r}\left(r\frac{\partial C}{\partial r}\right) + \frac{D^*}{Pe^2}\frac{\partial^2 C}{\partial z^2}, \tag{12}$$

$$D^* = \begin{Bmatrix} D_p & \text{in } \mathcal{R}_p \\ D_c & \text{in } \mathcal{R}_c \\ 1 & \text{in } \mathcal{R}_n \end{Bmatrix}, \tag{13}$$

along with initial and boundary conditions

$$\left.\begin{aligned} C(0,r,z) &= B(r)\psi(z), \quad (0 < r < 1) \\ \psi(z) &= \frac{\delta(z)}{Pe} \\ B(r) &= 1 \end{aligned}\right\}, \tag{14}$$

$$\frac{\partial C}{\partial r} = 0 \quad \text{at} \quad r = 0, \tag{15}$$

$$\frac{\partial C}{\partial r} = -\beta C \quad \text{at} \quad r = 1. \tag{16}$$

Here C_0 is the initial concentration of the slug input, u_0 is the time-averaged axial velocity, β is the absorption parameter or first order reaction rate representing the rate of loss on the wall. *Pe* is the Peclet number which measures the relative characteristic time of the diffusion process $\left(\frac{R^2}{D_n}\right)$ to the convection process $\left(\frac{R}{u_0}\right)$. *Sc* is the Schmidt number which is the ratio of viscous diffusion to the molecular diffusion. The dimensionless frequency parameter α is known as the Womersely frequency parameter which is the ratio of transient inertial force to viscous force. The radius of the cylinder containing the solute to that of the entire tube is assumed as value one, subsequently, the slug initially occupies the entire cross section of the tube.

IV. VELOCITY DISTRIBUTION

The presence of non-linearity in the governing equations and the constitutive equations that are coupled together prevents one from getting an exact solution. Since the Schmidt number (*Sc*) is very large [$O(10^3)$] in arterial blood flows,[12] the parameter $\epsilon\ \left(=\frac{1}{Sc}\right)$ is very small. Thus, in the present study, we solve the linear momentum equations by a regular perturbation technique by considering ϵ as the perturbation parameter. The velocity distributions in the three different layers are given by (the details are provided in Appendix A)

$$\begin{aligned} u_{cp}(r,t) = \frac{p(t)}{m}\Bigg[& m(1-R_o^2) + R_o^2\Bigg\{1 - \xi_2^2 - \frac{4\sqrt{2}}{3}\xi_2^{\frac{1}{2}}\left(1-\xi_2^{\frac{3}{2}}\right) \\ & + \xi_2(1-\xi_2)\Bigg\}\Bigg] + \frac{\epsilon\, p'(t)}{16}\Bigg[\frac{n}{m}R_o\,\log(R_o)\{8\,m\,R_o \\ & \times(1-R_o^2) + R_o^3\left(4 - \frac{16\sqrt{(2\xi_2)}}{7}\right)\Bigg\} - R_o^4 + 4R_o^2 - 3 \\ & - 4R_o^2\,(2-R_o^2)\,\log(R_o) - \frac{4n}{m}R_o^2(1-R_o^2)(1-\xi_2^2) \\ & - \frac{n}{m^2}R_o^4\Bigg\{3 - \frac{32\sqrt{2\xi_2}}{3}\left(\frac{33}{196} - \frac{\xi_2^2}{4} + \frac{4}{49}\xi_2^{\frac{7}{2}}\right) \\ & - 4\xi_2^2 + \xi_2^4\Bigg\} + \frac{16}{3\sqrt{2}}\frac{n}{m}R_o^2(1-R_o^2)\left(1-\xi_2^{\frac{3}{2}}\right) \\ & + \frac{16R_o^4 n}{\sqrt{2}m^2}\sqrt{\xi_2}\Bigg\{\frac{11}{42} - \xi_2^{\frac{1}{2}}\,\frac{2\sqrt{2}}{3}\left(\frac{5}{21} - \frac{1}{3}\xi_2^{\frac{3}{2}} + \frac{2}{21}\xi_2^3\right) \\ & - \frac{1}{3}\xi_2^{\frac{3}{2}} + \frac{1}{14}\xi_2^{\frac{7}{2}}\Bigg\}\Bigg], 0 \le r \le R_p \end{aligned} \tag{17a}$$

$$\begin{aligned} u_c(r,t) = \frac{p(t)}{m}\Bigg[& m(1-R_o^2) + R_o^2\Bigg\{1 - \xi_1^2 - \frac{4\sqrt{2}}{3}\xi_2^{\frac{1}{2}} \\ & \times\left(1-\xi_1^{\frac{3}{2}}\right) + \xi_2(1-\xi_1)\Bigg\}\Bigg] + \frac{\epsilon\, p'(t)}{16}\Bigg[\frac{n}{m}R_o\log(R_o) \\ & \times\Bigg\{8\,m\,R_o(1-R_o^2) + R_o^3\left(4 - \frac{16\sqrt{(2\xi_2)}}{7}\right)\Bigg\} - R_o^4 \\ & + 4R_o^2 - 3 - 4R_o^2\,(2-R_o^2)\log(R_o) \\ & - (4n/m)R_o^2(1-R_o^2)(1-\xi_1^2) - \frac{n}{m^2}R_o^4 \\ & \times\Bigg\{3 - \frac{32\sqrt{2\xi_2}}{3}\left(\frac{33}{196} - \frac{\xi_1^2}{4} + \frac{4}{49}\xi_1^{\frac{7}{2}}\right) - 4\xi_1^2 + \xi_1^4\Bigg\} \\ & + \frac{16}{3\sqrt{2}}\frac{n}{m}R_o^2(1-R_o^2)\left(1-\xi_1^{\frac{3}{2}}\right) + \frac{16R_o^4 n}{\sqrt{2}m^2}\sqrt{\xi_2} \\ & \times\Bigg\{\frac{11}{42} - \xi_2^{\frac{1}{2}}\frac{2\sqrt{2}}{3}\left(\frac{5}{21} - \frac{1}{3}\xi_1^{\frac{3}{2}} + \frac{2}{21}\xi_1^3\right) \\ & - \frac{1}{3}\xi_1^{\frac{3}{2}} + \frac{1}{14}\xi_1^{\frac{7}{2}}\Bigg\}\Bigg], R_p \le r \le R_o \end{aligned} \tag{17b}$$

$$u_n(r,t) = p(t)(1-r^2) + \frac{\epsilon\, p'(t)}{16}\left[\frac{n}{m} R_o \log(r)\left\{8\, m\, R_o(1-R_o^2) + R_o^3\left(4 - \frac{16\sqrt{2\xi_2}}{7}\right)\right\} - r^4 + 4r^2 - 3 - 4R_o^2 \times (2 - R_o^2)\log(r)\right]. \qquad R_o \le r \le 1 \tag{17c}$$

The velocity distributions of shear flow in the Casson and Newtonian regions are given by u_c and u_n, respectively. The constant velocity u_{cp} appears only in the plug flow region having radius $R_p = \frac{\tau_y}{p(t)}$ (plug core radius), where $p(t) = \left(1 + e\sin(\alpha^2\, Sc\, t)\right)$; $e = \frac{A_1}{A_0}$ is the amplitude of the fluctuating pressure component, α is the Womersely frequency parameter, and Sc is the Schmidt number. The term Ω $(=\alpha^2\ Sc\ t)$ is known as the phase angle of pressure pulsation. The quantity R_0 (≤ 1) is the ratio of the central core radius to normal pipe radius. Small values of R_o signify a large peripheral layer region, where γ $(=[1-R_o])$ is known as the peripheral layer thickness. If $R_o = 1$ or $\gamma = 0$, the model will be a single-fluid Casson model. Here m is the viscosity ratio, which indicates the influence of the Casson viscosity (μ_c) compared to the Newtonian viscosity (μ_n) and n is the density ratio indicating the influence of Casson density (ρ_c) compared to the Newtonian density (ρ_n) within the layered liquid regime.

V. ARIS-BARTON APPROACH

The pth moment of the distribution of the solute in the direction of flow can be described by Aris-Barton[8] as

$$C^{(p)}(t,r) = \int_{-\infty}^{+\infty} z^p C(t,r,z)dz. \tag{18}$$

Using Eq. (18), the diffusion Eq. (12) subject to the initial and boundary conditions (14)–(16) can be written as

$$\frac{\partial C^{(p)}}{\partial t} - \frac{D^*}{r}\frac{\partial}{\partial r}\left(r\frac{\partial C^{(p)}}{\partial r}\right) = p\, u(r,t)\, C^{(p-1)} + \frac{D^*}{Pe^2}p(p-1)C^{(p-2)}, \tag{19}$$

with

$$\left.\begin{aligned} C^{(p)}(0,r) &= \begin{cases} \frac{1}{Pe} & \text{for } p = 0 \\ 0 & \text{for } p > 0 \end{cases} \\ \frac{\partial C^{(p)}}{\partial r} &= 0 \quad \text{at} \quad r = 0, \\ \frac{\partial C^{(p)}}{\partial r} &= -\beta C^{(p)} \quad \text{at} \quad r = 1, \end{aligned}\right\}. \tag{20}$$

The cross-sectional average of the pth moment of the distribution of the solute is given by

$$\left\langle C^{(p)}(t)\right\rangle = \frac{1}{\pi}\int_0^{2\pi} d\theta \int_0^1 rC^{(p)}(t,r)dr, \tag{21}$$

where $\langle\ .\ \rangle$ denotes the cross-sectional mean.

With this definition, Eq. (19) and the conditions given in Eq. (20) become

$$\frac{\mathrm{d}}{\mathrm{d}t}\left\langle C^{(p)}\right\rangle + 2\beta D^* C^{(p)}(t,1) = p\left\langle u(r,t)C^{(p-1)}\right\rangle + \frac{D^*}{Pe^2}\, p(p-1)\left\langle C^{(p-2)}\right\rangle, \tag{22}$$

with the initial condition

$$\left\langle C^{(p)}(0)\right\rangle = \begin{cases} \frac{1}{Pe} & \text{for p = 0} \\ 0 & \text{for p > 0.} \end{cases} \tag{23}$$

The pth order central moment about mean of the concentration distribution can be defined as

$$\mu_p(t) = \frac{\int_0^1\int_0^{2\pi}\int_{-\infty}^{+\infty} r(z-z_g)^p C\mathrm{d}r\mathrm{d}\theta\mathrm{d}z}{\int_0^1\int_0^{2\pi}\int_{-\infty}^{+\infty} rC\mathrm{d}r\mathrm{d}\theta\mathrm{d}z}, \tag{24}$$

where

$$z_g = \frac{\iiint zC\mathrm{d}v}{\iiint C\mathrm{d}v} = \frac{\left\langle C^{(1)}\right\rangle}{\left\langle C^{(0)}\right\rangle}$$

represents the "centroid" or "first moment" of the distribution of the solute and $\langle C^{(0)}\rangle$ is the total mass of the chemical species in the flowing stream.

The expressions for central moments can be obtained from Eq. (24) (see Appendix B) as

$$\left.\begin{aligned} \mu_2(t) &= \frac{\left\langle C^{(2)}\right\rangle}{\left\langle C^{(0)}\right\rangle} - z_g^2, \\ \mu_3(t) &= \frac{\left\langle C^{(3)}\right\rangle}{\left\langle C^{(0)}\right\rangle} - 3z_g\mu_2 - z_g^3, \\ \mu_4(t) &= \frac{\left\langle C^{(4)}\right\rangle}{\left\langle C^{(0)}\right\rangle} - 4z_g\mu_3 - 6z_g^2\mu_2 - z_g^4, \end{aligned}\right\}. \tag{25}$$

The second central moment, μ_2, represents the variance of the distribution about the mean position whose rate of change gives the dispersion coefficient. Following Aris,[5] the apparent dispersion coefficient, D_a, can be expressed as

$$D_a = \frac{1}{2}\frac{d\mu_2}{dt}, \tag{26}$$

where dispersion coefficient D_a depends on wall absorption parameter β, yield stress τ_y, peripheral layer thickness γ, viscosity ratio m, density ratio n, amplitude of the fluctuating pressure component e, Womersely frequency parameter α, etc. The coefficients of skewness ν_2 $(=\mu_3/\mu_2^{\frac{3}{2}})$ and kurtosis ν_3 $(=\mu_4/\mu_2^2 - 3)$ are important factors for measuring the degree of symmetry and peakedness of the concentration distribution, respectively.

VI. FINITE DIFFERENCE OF THE UNSTEADY CONVECTIVE DIFFUSION EQUATION IN THE THREE-LAYER REGION TO OBTAIN DISPERSION COEFFICIENT

To avoid the complexity of the analytical solution of moment equations (for p > 1) subject to the initial and boundary conditions, a standard finite difference method based on the Crank-Nicolson implicit scheme has been adopted to solve the set of integral moment equations. For this purpose, we divide the whole width of the pipe into $(M-1)$ equal parts having length Δr. The length and times are represented by the grid points j and i, respectively, so that the general formulas are $r_j = (j-1)\times\Delta r$ and $t_i = \Delta t\times(i-1)$. Here, $j = 1$, M correspond to the axis of the pipe $(r = 0)$ and the wall $(r = 1)$ of the pipe, respectively, also as $i = 1$ corresponds to the initial

time ($t = 0$), where Δt and Δr are the augmentations of t and r, respectively. $C^{(p)}$ (i, j) indicates the value of $C^{(p)}$ at the ith grid point along the t-axis and jth grid point along the r-axis. The resulting finite difference formula leads to a system of algebraic equation with a tri-diagonal coefficient matrix, given by

$$P_j C^{(p)}(i+1, j+1) + Q_j C^{(p)}(i+1, j) + R_j C^{(p)}(i+1, j-1) = S_j, \tag{27}$$

where P_j, Q_j, R_j, and S_j are the matrix elements. The finite difference form of the initial condition is

$$\begin{aligned} C^{(p)}(1, j) &= \tfrac{1}{Pe}, \quad \text{for} \quad p = 0 \\ &= 0, \quad \text{for} \quad p > 0 \end{aligned} \tag{28}$$

and that of boundary conditions are

$$\begin{aligned} &C^{(p)}(i+1, 0) = C^{(p)}(i+1, 2), \text{at the axis of pipe,} \\ &\text{and} \\ &C^{(p)}(i+1, M+1) = C^{(p)}(i+1, M-1) \\ &\qquad\qquad - 2\Delta r \beta C^{(p)}(i+1, M), \\ &\text{at the surface of the pipe wall.} \end{aligned} \tag{29}$$

A MATLAB code has been developed to solve the tri-diagonal coefficient matrix for Eqs. (27)–(29) by the Thomas algorithm.[4] The computation steps are as follows:
Step-1: The time dependent axial velocity u is computed first from Eqs. (17a)–(17c).
Step-2: The concentration $C^{(p)}$ is then calculated from Eq. (19) as the value of $u(r, t)$ at each of the grid points are known from *step-1*.
Step-3: Finally the value of $\langle C^{(p)} \rangle$ is calculated from Eq. (21) by Simpson's one-third rule, using the values obtained from *step-1* and *step-2* at the corresponding grid points.

Numerical calculations have been performed to discuss individual dispersion processes due to absorption parameter, yield stress, peripheral layer thickness, viscosity ratio, density ratio, amplitude of fluctuating pressure component, Womersely frequency parameter, and molecular diffusivity at different layers. The present scheme is linearly stable for any finite values of $\Delta t/(\Delta r)^2$, where a mesh size ($\Delta t = 0.000\,01, \Delta r = 1/(M-1)$) and $M = 100$, gives satisfactory results for different values of parameters. In all the cases, we have taken $Sc = Pe = 10^3$. By varying the time step and grid spacings, we have assured a very good order of accuracy of the results generated by the above-mentioned spatial and temporal discretization parameters. Actually, the smaller time interval is needed to trap the oscillatory nature in the dispersion process. Sufficiently small spatial discretization has been utilized in order to keep the accuracy of the results.

VII. CALCULATION OF THE NON-GAUSSIAN MEAN SOLUTE CONCENTRATION USING HERMITE POLYNOMIALS

The behaviour of concentration distribution might also be acquired from the information of the first four central moments of the distribution. Utilizing these four moments, it is possible to approximate the mean axial concentration distribution $C_m(z, t)$ of tracers within the flow region with the assistance of Hermite polynomial representation for non-Gaussian curves[30] and is given by

$$C_m(z, t) = \left\langle C^{(0)}(t) \right\rangle e^{-\eta^2} \sum_{n=0}^{\infty} a_n(t) H_n(\eta), \tag{30}$$

where $\eta = (z - z_g)/\sqrt{2\mu_2}$, $z_g = \frac{\langle C^{(1)} \rangle}{\langle C^{(0)} \rangle}$ and H_i, the Hermite polynomials, satisfy the recurrence relation with $H_0(\eta) = 1.0$ as

$$H_{i+1}(\eta) = 2\eta H_i(\eta) - 2i H_{i-1}(\eta), \quad i = 0, 1, 2, \ldots.$$

The coefficients a_i's are

$$a_0 = 1/(2\pi\mu_2)^{1/2}, \; a_1 = a_2 = 0,$$
$$a_3 = 2^{1/2} a_0 \nu_2/24, \; a_4 = a_0 \nu_3/96.$$

Therefore, given the statistical parameters in Eq. (25), the concentration distribution can be estimated from Eq. (30) at any given location in the axial direction and time.

VIII. RESULTS AND DISCUSSION

In order to study the solute dispersion in the laminar flow of a layered liquid with wall reaction, a pulsatile nature of the Poiseuille flow is considered due to its versatile applications in physiological fluid dynamics. Inline with the discussions outlaid in Sec. I, the importance of the effect of the peripheral layer in blood flow, the values of yield stress and peripheral layer thickness assume a pivotal significance. In contrast to existing studies in this direction, the present study has investigated the parametric effect of molecular diffusivity at different liquid layers which has helped one to project the importance of viscosity and density ratios in the present paradigm of the study. In order to establish the desired parametric effect in both qualitatively and quantitatively, the ranges of the values of parameters considered in the study are provided in Table II.

The variations of the velocity distribution due to non-Newtonian flow characteristic parameter or yield stress τ_y, viscosity ratio m, density ratio n, and peripheral layer thickness γ are shown in Fig. 2, when phase angles Ω are $\frac{3\pi}{4}$ and $\frac{5\pi}{4}$, respectively. Figures 2(a) and 2(b) show that velocity is decreased with the increment of both τ_y and m whereas, a non-uniform behaviour is experienced for n which can be seen from Fig. 2(c). Figure 2(d) clearly shows that velocity is

TABLE II. Values of parameter relevant to physiologically blood flows of human circulatory system.

Parameter	Range of value
τ_y, yield stress[16,35]	0 – 0.1
γ, peripheral layer thickness[41,43]	0 – 0.2
α, Womersely frequency parameter[35]	0.05 – 0.5
e, fluctuating pressure component[32,41]	0 – 1
m, viscosity ratio[43]	1 – 2
n, density ratio[29]	1 – 1.09

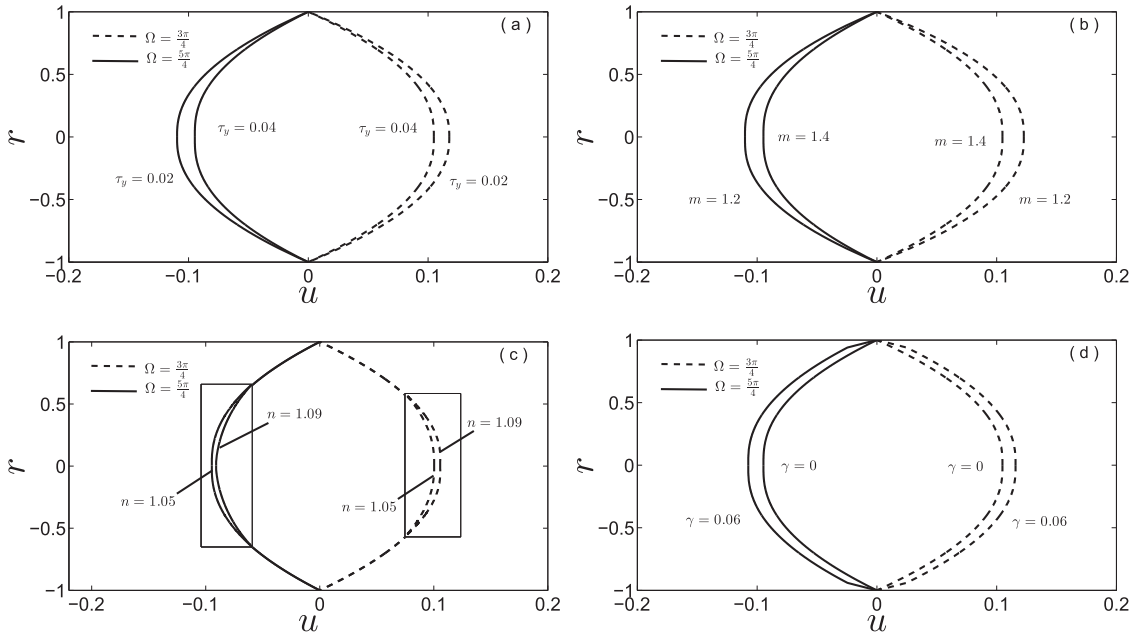

FIG. 2. Profiles of the unsteady component of velocity for different values of (a) yield stress τ_y, (b) viscosity ratio m, (c) density ratio n, and (d) peripheral layer thickness γ, when the phase angle of pressure pulsation is $\Omega = \frac{3\pi}{4}$ and $\frac{5\pi}{4}$.

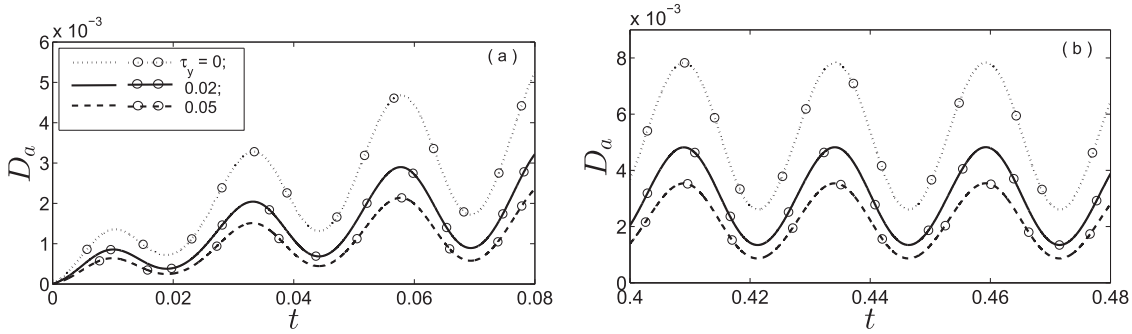

FIG. 3. Variation of dispersion coefficient D_a with time t for different values of yield stress τ_y, when $\beta = 0.01$, $\alpha = 0.5$, $e = 0.5$, and $Sc = 1000$. (a) For small times; (b) for large times (curved lines with circles are the results of the work of Rana and Murthy[35]).

decreased by small γ. A similar kind of behaviour is observed by Sankar and Lee,[41] the resistance to the flow for the two-fluid model is considerably less than that of the single-fluid model.

To solve the integral moment equations, a MATLAB code has been prepared based on the standard finite difference Crank-Nicolson implicit scheme. The accuracy of the numerical scheme has been justified from the following cases:

Case-I: In order to compare the results of dispersion obtained in the present study with those established by Rana and Murthy,[35] the parameters under a periodic pressure gradient has been characterized by the same values of $\gamma = 0$, $D_p = D_c = 1$, $m = n = 1$, and $\beta = 0.01$, etc. Figures 3(a) and 3(b) show the temporal variation of the dispersion coefficient with yield stress τ_y. As is evident from the results obtained, the model trend completely concurs qualitatively and quantitatively with that obtained in the study of Rana and Murthy.[35] (see Fig. 3 totally coincides with Fig. 11 in Ref. 35).

Case-II: In order to validate the present model with the results established in the study of Dash *et al.*,[17] the simulation parameters of D_p, D_c, m, and n bearing their individual significance have been kept at unity and $\gamma = 0$, etc. To this end,

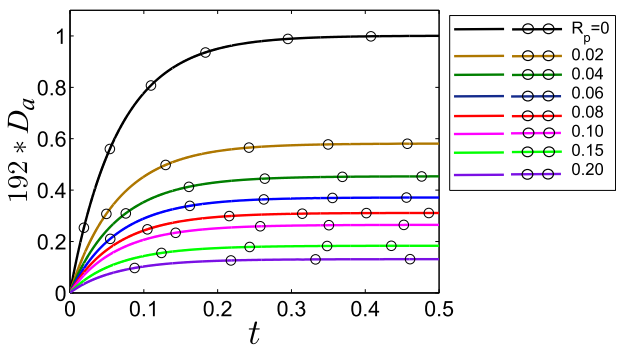

FIG. 4. Variation of dispersion coefficient ($192 \times D_a$) with t for various values of plug radius (R_p) (curved lines with circles are the results of the work of Dash *et al.*[17]).

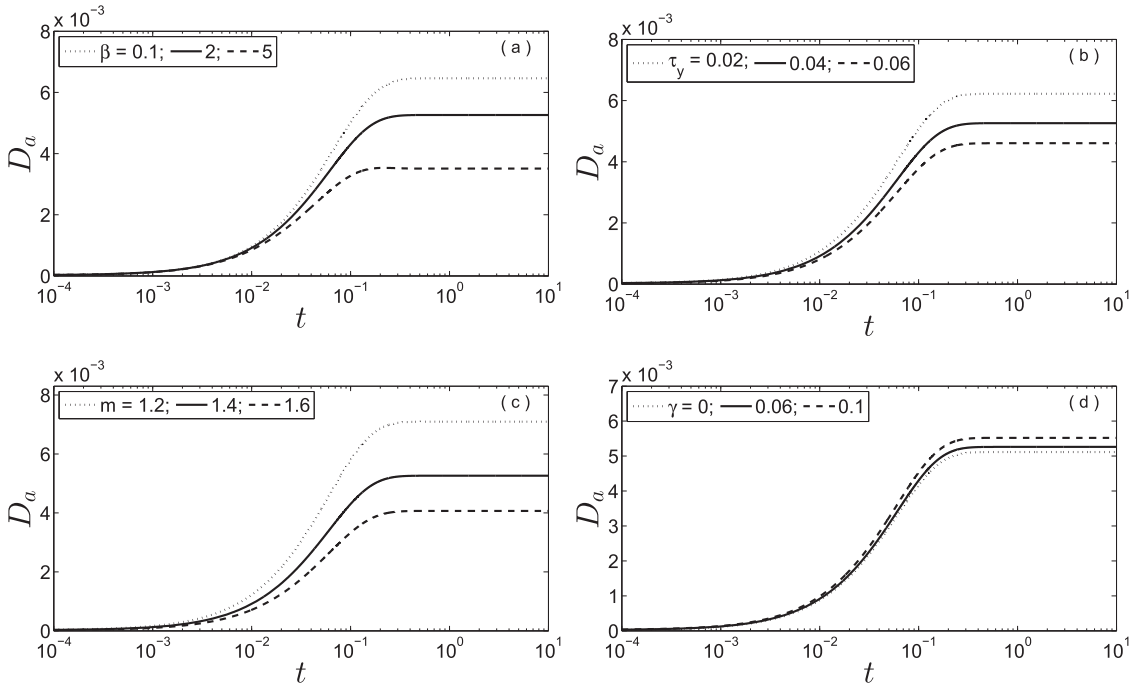

FIG. 5. For steady flow, time assessment of dispersion coefficient for fixed $e = 0$, $D_p = D_c = 1$, (a) variation of absorption parameter (β) when $m = 1.4$, $\tau_y = 0.04$, and $\gamma = 0.06$; (b) variation of yield stress (τ_y) when $m = 1.4$, $\beta = 2$, and $\gamma = 0.06$; (c) variation of viscosity ratio (m) when $\tau_y = 0.04$, $\beta = 2$, and $\gamma = 0.06$; (d) variation of peripheral layer thickness (γ) when $m = 1.4$, $\tau_y = 0.04$, and $\beta = 2$.

the response of the model, outlaid in Fig. 4, displays complete agreement with the work of Dash *et al.*[17] in the absence of catalytic wall reaction, i.e., $\beta = 0$ [see Fig. 4 totally coincides with Fig. 2(a) in Ref. 17].

From the above cases (Figs. 3 and 4), it is noticeable that as the non-Newtonian effect or plug flow radius increases, both the amplitude of fluctuations and the magnitude of the dispersion coefficient decrease for all time. Higher values of non-Newtonian parameter lead to the increase of flow resistance, strictly diminishing the value of the dispersion coefficient. In both the cases of steady or unsteady flows, initially, dispersion coefficient is the increasing function of time whereas after a fixed value of time, D_a becomes constant or uniform.

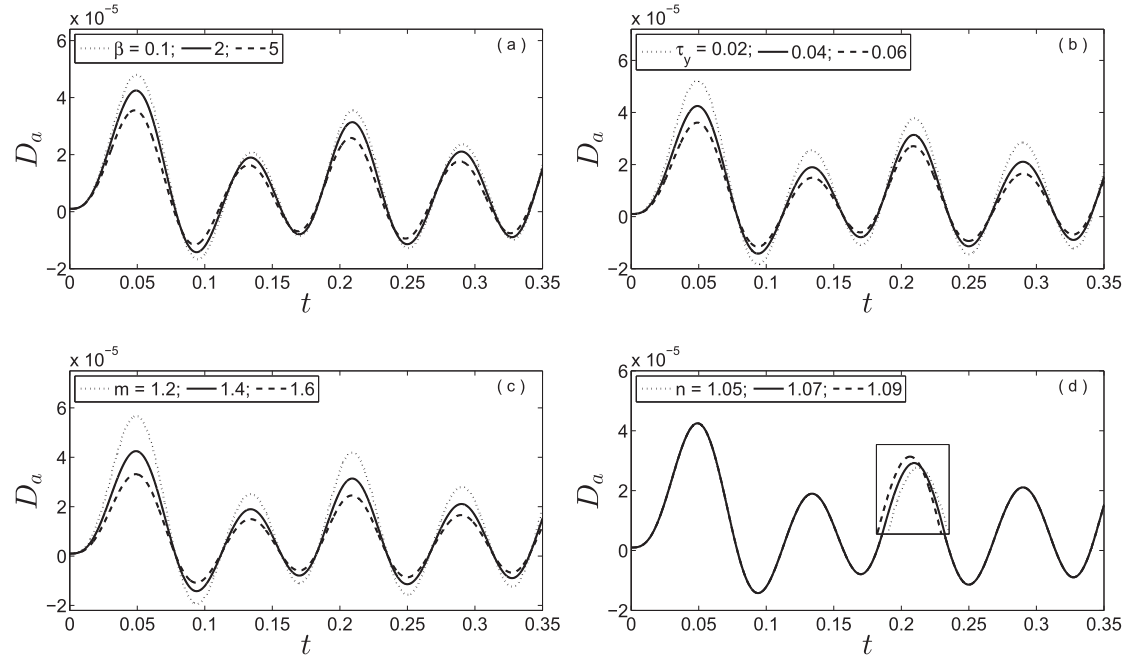

FIG. 6. For unsteady flow, time assessment of dispersion coefficient for fixed $\gamma = 0.06$, $e = 0.3$, $\alpha = 0.2$, $D_p = D_c = 1$, at small time interval; (a) variation of absorption parameter (β) when $m = 1.4$, $n = 1.07$, and $\tau_y = 0.04$; (b) variation of yield stress (τ_y) when $m = 1.4$, $n = 1.07$, and $\beta = 2$; (c) variation of viscosity ratio (m) when $n = 1.07$, $\tau_y = 0.04$, and $\beta = 2$; (d) variation of density ratio (n) when $m = 1.4$, $\tau_y = 0.04$, and $\beta = 2$.

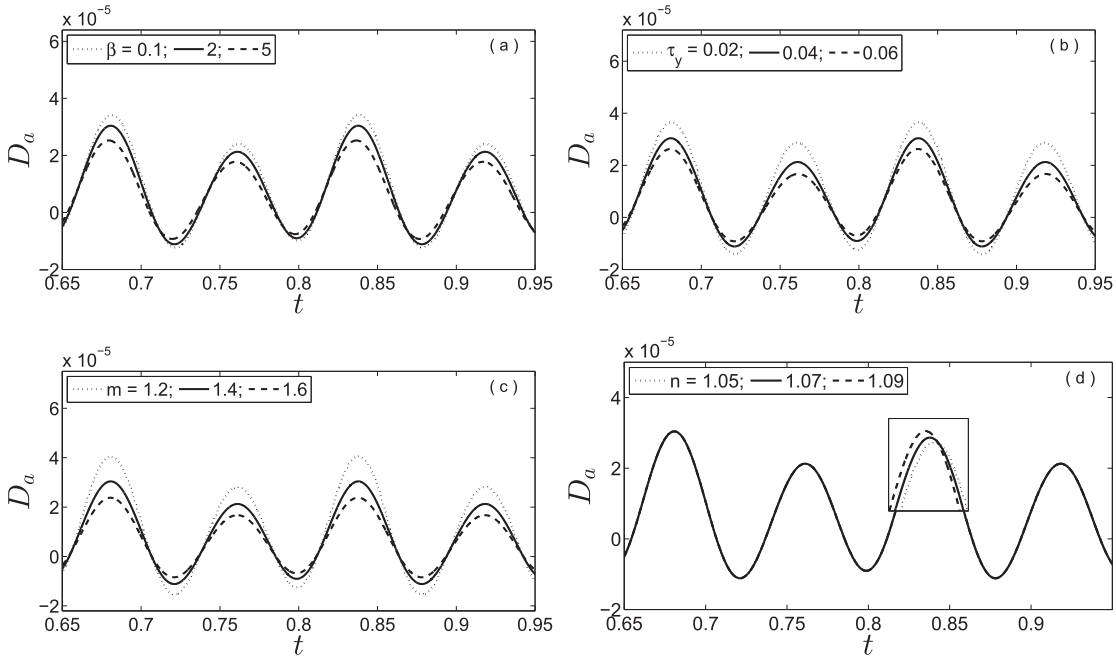

FIG. 7. Same as Fig. 6 but at large time.

Variation of dispersion coefficient D_a with respect to time t is shown in Fig. 5 for steady flow with different values of the absorption parameter β, yield stress τ_y, viscosity ratio m, and peripheral layer thickness γ, respectively. A wide range of time is considered to track the asymptotic approach of the dispersion coefficient. Profile in Fig. 5(a) represents the behaviour of D_a for various values of β where the increase in β leads to the decrease in D_a. Initially, it is found that the magnitude of D_a increases with time for every values of β, though after a large time, D_a reaches to constant values 6.461×10^{-3}, 5.257×10^{-3}, and 3.532×10^{-3} for $\beta = 0.1,\ 2$, and 5 when $t = 0.5441$, 0.3959, and 0.213, respectively. Hence, the time required for steady state is decreased with wall absorption. The physical perception about the decrement of D_a with increasing β leads to an increase in the quantity of moles of reactive material undergoing chemical reaction or absorption resulting a change in the concentration distribution across the tube with the simultaneous consequence of a drop in dispersion coefficient. Figure 5(b) is drawn to emphasize the effect of τ_y on D_a in order to highlight the pivotal significance of low shear rate applicable to blood flow through small blood vessels in the presence of a peripheral layer. It is observed

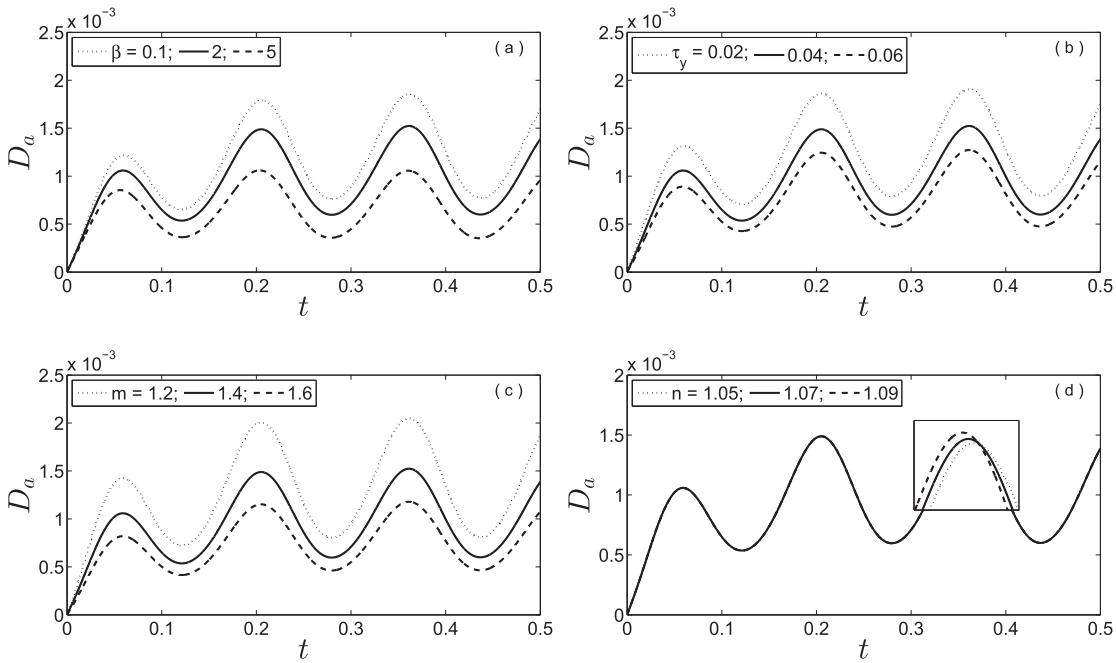

FIG. 8. For combined flow, time assessment of dispersion coefficient in a three-layer liquid flow in a small time interval. Others description are as in Fig. 6.

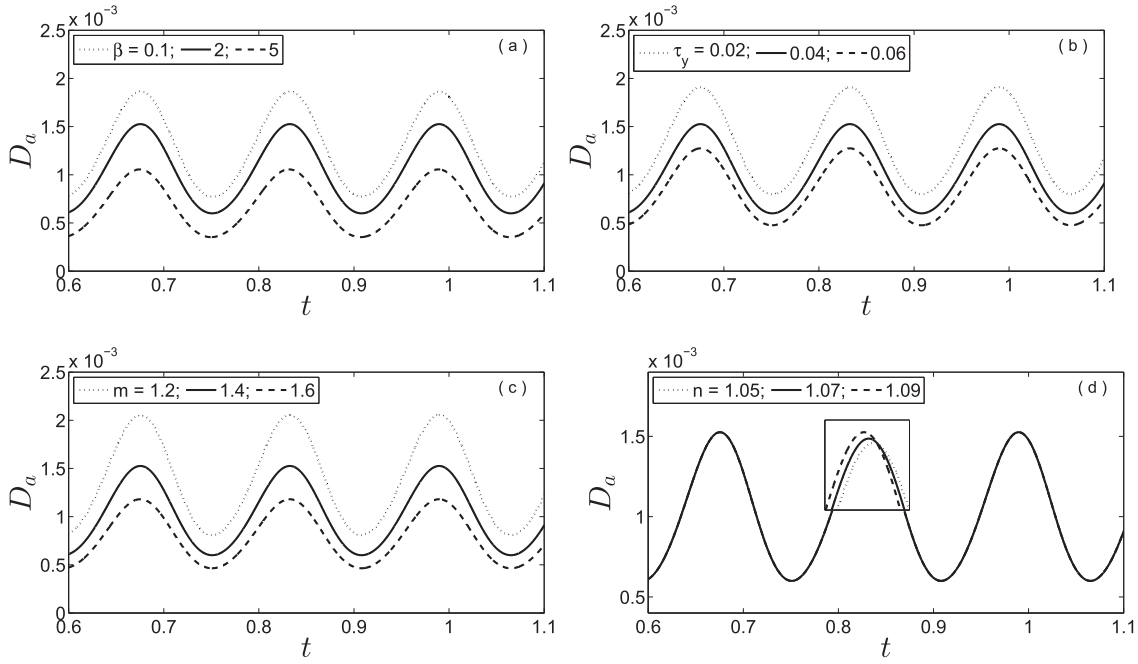

FIG. 9. Same as Fig. 8 but at large time.

that the dispersion coefficient decreases with the increase in yield stress, as the increase in the non-Newtonian parameter decreases the velocity of the liquid. Viscosity ratio m is the ratio of Casson viscosity μ_c to Newtonian viscosity μ_n; and density ratio n is defined as the ratio of Casson density ρ_c to Newtonian density ρ_n. The main advantage of using m and n on the study of dispersion is that it directly discloses how strong is the influence of μ_c and ρ_c compared with μ_n and ρ_n. For a steady flow, dispersion coefficient D_a is independent of density ratio n which can also be concluded from Eqs. (17a)–(17c) for $e = 0$. The time evaluation of dispersion coefficient D_a under the effect of m has been projected in Fig. 5(c). As can be inferred from Fig. 5(c), we can observe that D_a increases with time t for a short period beyond which it attains a steady state. Again, as m increases, the magnitude of D_a decreases. This happens in light of the fact that the increment of m causes a decrease in velocity distribution. From Fig. 5(d), one can easily observe that the increase in the peripheral layer thickness leads to a significant augmentation of dispersion coefficient.

When the flow is purely oscillatory, time variation of dispersion coefficients is shown in Fig. 6, and in Fig. 7, for small and large time, respectively. During small as well as large time, Figs. 6(a) and 7(a) show that the dispersion coefficient decreases with the increase in the absorption parameter β which is associated with the irreversible reaction on the tube wall. A similar kind of behaviour of dispersion under absorption has been followed and reasoned by Mazumder and Das.[25] The rheology of blood is strongly influenced by yield stress τ_y which imparts various qualities to a fluid as indicated by McDonald.[28] According to Krishnan *et al.*,[22] the yield stress values for normal human blood is between 0.01 and 0.06 dyn/cm^2. Figures 6(b) and 7(b) show that yield stress inhabits the dispersion process for all time. The reason of such behaviour is due to weak stream produced by high yield stress

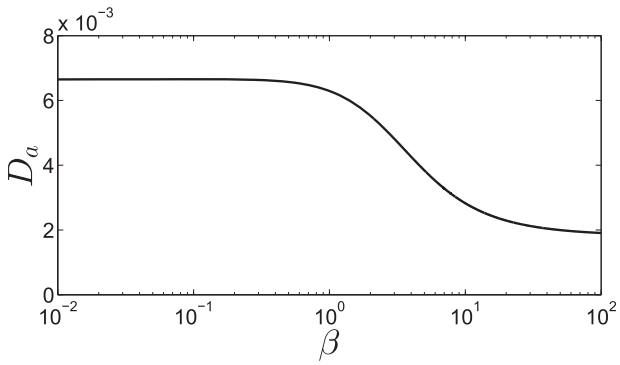

FIG. 10. Variation of dispersion coefficient D_a with absorption rate β for a fixed time $t = 0.5$, when $\gamma = 0.06$, $e = 0$, $\tau_y = 0.04$, $m = 1.4$.

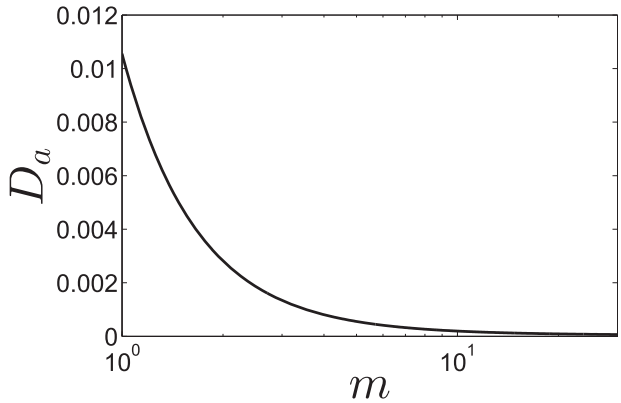

FIG. 11. Variation of dispersion coefficient with viscosity ratio m for a fixed time $t = 0.5$, when $\gamma = 0.06$, $e = 0$, $\tau_y = 0.04$, $\beta = 2$.

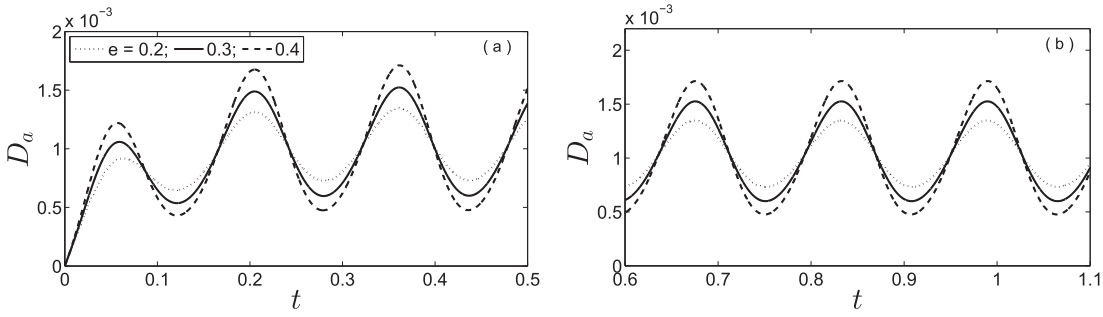

FIG. 12. For combined flow, time assessment of dispersion coefficient with the variation of amplitude of the fluctuating pressure component e when $\beta = 2$, $m = 1.4$, $n = 1.07$, $\tau_y = 0.04$, $\gamma = 0.06$, $\alpha = 0.2$, $D_p = D_c = 1$; (a) for small times; (b) for large times.

at the carrier flow. It can be seen from Fig. 6(c) that, like the case of steady flow, dispersion coefficient shows a decreasing trend with the increase in the viscosity ratio m. The behaviour of the dispersion coefficient is not uniform with respect to the density ratio n, which has been captured in Fig. 6(d). The variation of D_a with respect to both m and n follows same individual trends for the large times also, which are supported by Figs. 7(c) and 7(d). For all time, results show that the dispersion process becomes faster with the density ratio. The reason behind this augmentation could be the density improvement in the Casson layer due to the increment of the density ratio.

For combined flow, variation of dispersion coefficient at small and large times is shown in Figs. 8 and 9, respectively. The arrangement of the figures is same as the previous figures. It can be easily detected from Figs. 8(a) and 9(a) that, for all time, the asymptotic values of D_a diminish as the absorption rate becomes faster. Initially the dispersion coefficient increases periodically with wavy nature, though after a critical time it reaches non-transient state. It is noticeable that, when the time is large, somewhat similar qualitative effects of the absorption parameter on the dispersion coefficient can be seen from Fig. 9(a), except that the response of the dispersion coefficient seems to be more sensitive at large time, i.e., at large time, effects are more pronounced. The decrease in the dispersion coefficient with the increase in the irreversible reaction parameter is based on sound physical ground which has already been discussed in the above paragraph. The effect of yield stress τ_y on dispersion coefficient D_a for a combined flow situation has been shown in Fig. 8(b) such that an increase in the non-Newtonian parameter leads to a decrease in the magnitude of D_a. More vivid effects of τ_y can be noticed in Fig. 9(b), though the qualitative nature of the dispersion coefficient remains the same as in initial time [Fig. 8(b)]. Nagarani and Sebastian[32] also obtained the same nature of the dispersion coefficient when yield stress τ_y was significant. The increase in the viscosity ratio also reduces the magnitude of the dispersion coefficient. Figure 8(c) shows that initially D_a is found to increase with time but after a fixed time, the fluctuation becomes more stable and finally reaches to a non-transient state [see Fig. 9(c)]. It has already been discussed that for the case of steady flow, D_a is independent of density ratio n. Figures 8(d) and 9(d) show the temporal variation of D_a with respect to n. An increase in density ratio makes a variable impact on the dispersion coefficient for small as well as large time intervals. As the density ratio increases, the relative axial velocity between the liquid layer increases or decreases depending on the phase angles. It should be mentioned here that the fall and growth of the dispersion coefficient with the variation of the parameters should not be taken as ultimate. The situation may differ depending on the strength of the reactions, span of time, frequency of pressure pulsation, etc. This fact can be partially realized later from Figs. 10–13.

For a steady flow situation, the relation of dispersion coefficient D_a with the irreversible reaction parameter β and viscosity ratio m for a fixed instant of time is, respectively, shown in Figs. 10 and 11. From Fig. 10, it is found that up to a certain small value of β, dispersion coefficient increases with it and after that critical value, dispersion coefficient shows a steep decrease with β and finally reaches to its asymptotic value when absorption is so high at the pipe boundary. So for weak boundary absorption, dispersion coefficient is in fact enhanced, i.e., the absorption parameter has an insignificant effect during the initial stage, for that span of time which is not sufficient for the absorption parameter to be fully activated. The result outlaid in Fig. 11 is the viscosity ratio effect on dispersion for a fixed time $t = 0.5$. It is shown in the figure that as the viscosity ratio increases, the value of the dispersion coefficient goes downward and eventually reaches a steady state position.

In Figs. 12 and 13, behaviour of D_a has been observed for different values of amplitude of the fluctuating pressure component e and Womersely frequency parameter α. It can be easily observed that, as e increases, both the amplitude

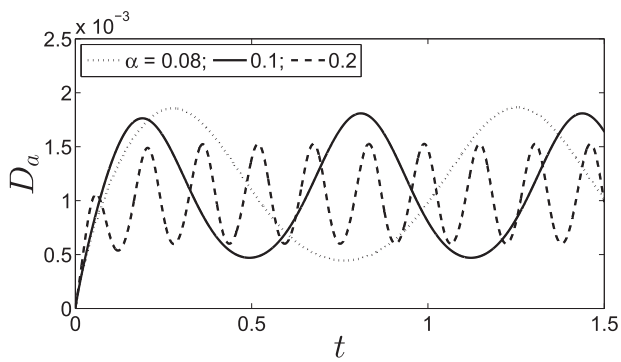

FIG. 13. For combined flow, time assessment of dispersion coefficient with the variation of Womersely frequency parameter α when $\beta = 2$, $m = 1.4$, $n = 1.07$, $\tau_y = 0.04$, $\gamma = 0.06$, $e = 0.3$, and $D_p = D_c = 1$.

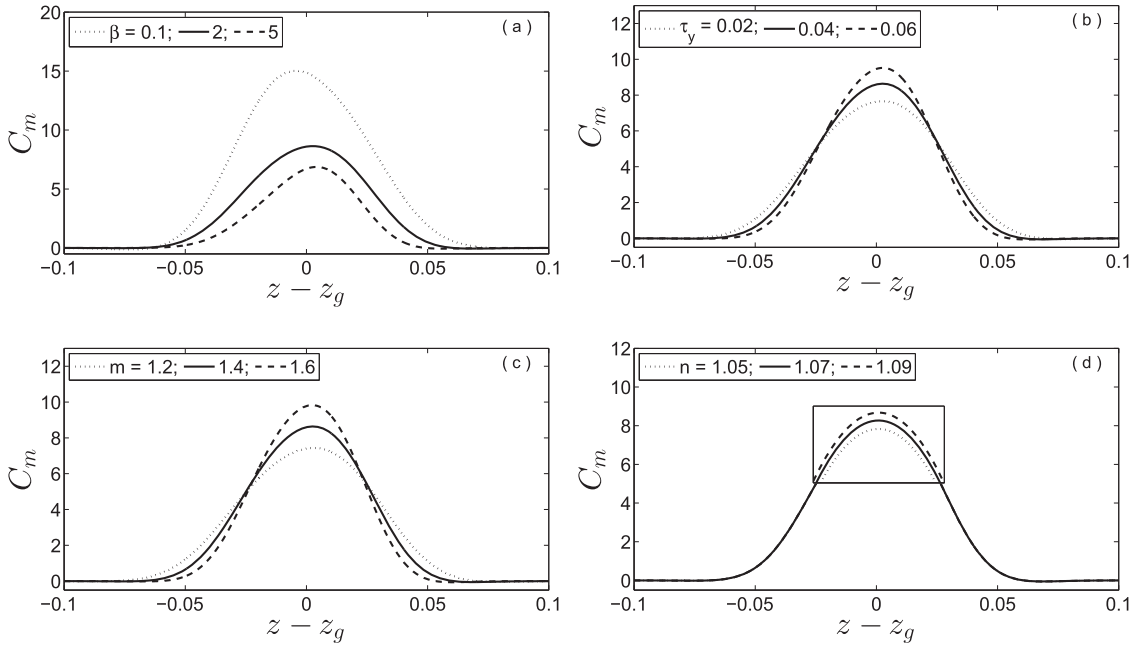

FIG. 14. Axial distribution of mean concentration for combined flows with different values of (a) absorption rate β, (b) yield stress τ_y, (c) viscosity ratio m, and (d) density ratio n at a fixed time, $t = 0.25$. Other descriptions are as in Fig. 6.

of fluctuations and the magnitude of D_a increase though the same are decreased due to high frequency parameter α. A similar kind of conclusion has been noticed and reasoned by Rana and Murthy[35] in their single phase Casson model. Under the consideration of both e and α, dispersion coefficient is increasing within the initial time interval; however, after a critical time, the flow pulsations become uniform. It should be noticed that the critical time of D_a to reach the non-transient stage is independent of e. From Fig. 13, it is seen that large values of the frequency parameter helps one to reach the non-transient state of D_a in the earlier time since the increase in the frequency parameter would decrease the period of oscillations.

Figures 14 and 15 present the investigation of mean concentration distribution across the axial distance for combined nature of stream at dimensionless times $t = 0.25$ and 0.5, respectively. Due to constant depletion occurring at the tube wall, the peak of the mean concentration decreases as absorption parameter β increases, shown in Figs. 14(a) and 15(a). It may become flat for large absorption, thus the

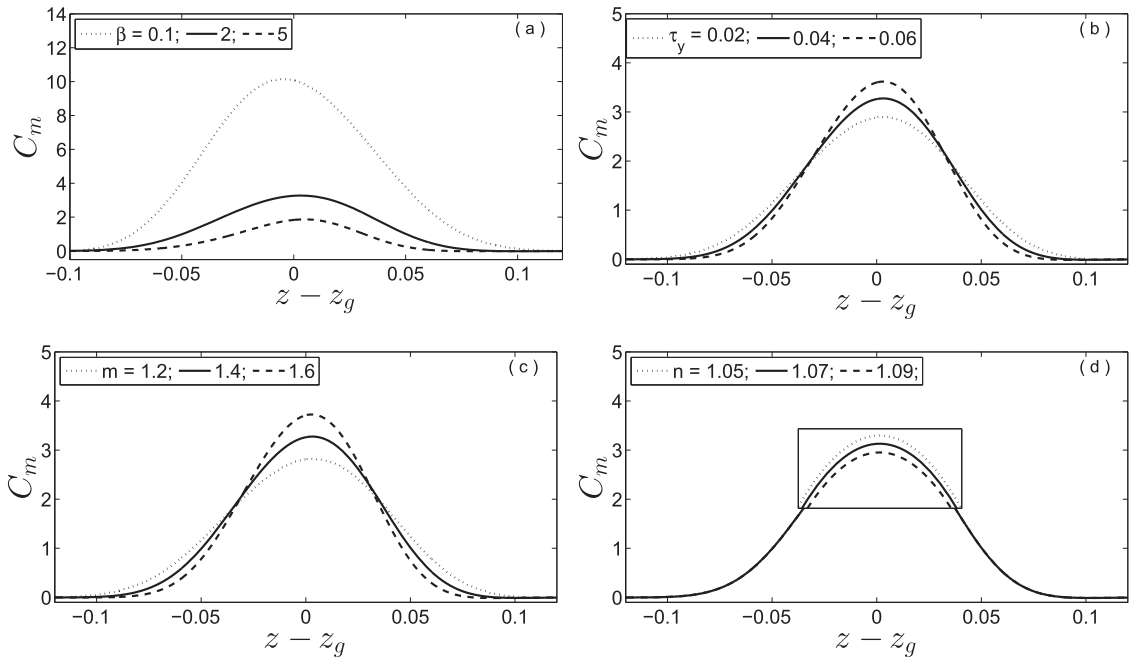

FIG. 15. Same as Fig. 14 but at time $t = 0.5$.

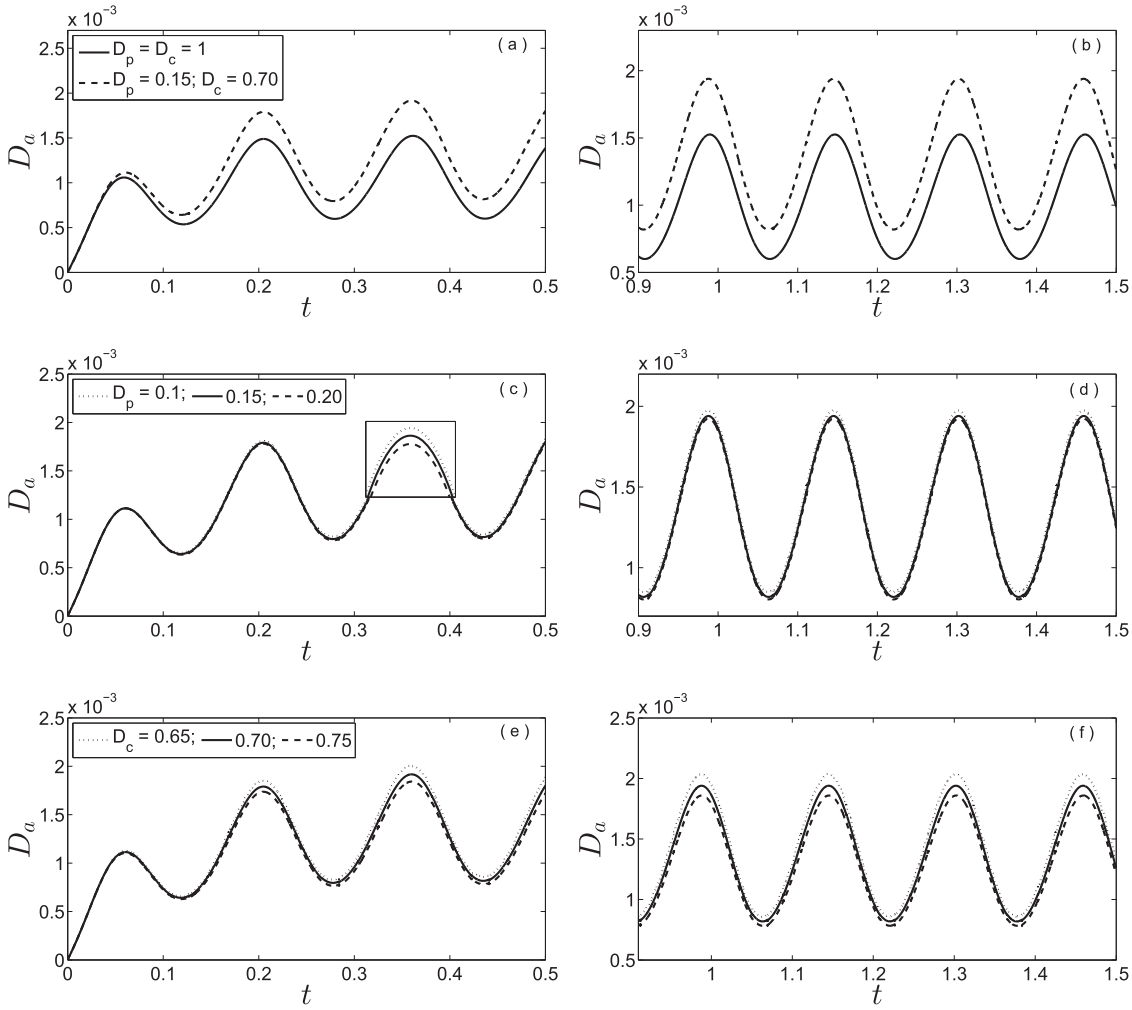

FIG. 16. For combined flow, time assessment of dispersion coefficient for various values of diffusivity when $\beta = 2$, $m = 1.4$, $n = 1.07$, $\tau_y = 0.04$, $\gamma = 0.06$, $e = 0.3$, $\alpha = 0.2$. (a) and (b) for $D_p = D_c = 1$, $D_p = 0.15$; $D_c = 0.70$, (c) and (d) for fixed $D_c = 0.70$ and (e) and (f) for fixed $D_p = 0.15$.

dispersion coefficient may not have practical importance for large absorption rate. While observing Figs. 14(b), 14(c), 15(b), and 15(c), it is found that as τ_y and m increase, the peak of the mean concentration distribution also increases. From Figs. 14(c) and 15(c), we have found that the mean of the concentration distributions is 7.436, 8.637, and 9.826 at time $t = 0.25$ and 2.821, 3.275, and 3.725 at time $t = 0.5$ when $m = 1.2$, 1.4, and 1.6, respectively. This indicates that the solute occupies increasingly greater portions of the cross-sectional area as m increases since the solute disperses through the low viscosity Newtonian liquid at a higher speed compared to the highly viscous Casson liquid. Like dispersion coefficient, axial distribution of mean concentration distribution also shows inhomogeneous behaviour with density ratio n. This fact can be realized through Figs. 14(d) and 15(d) at time $t = 0.25$ and 0.5, respectively.

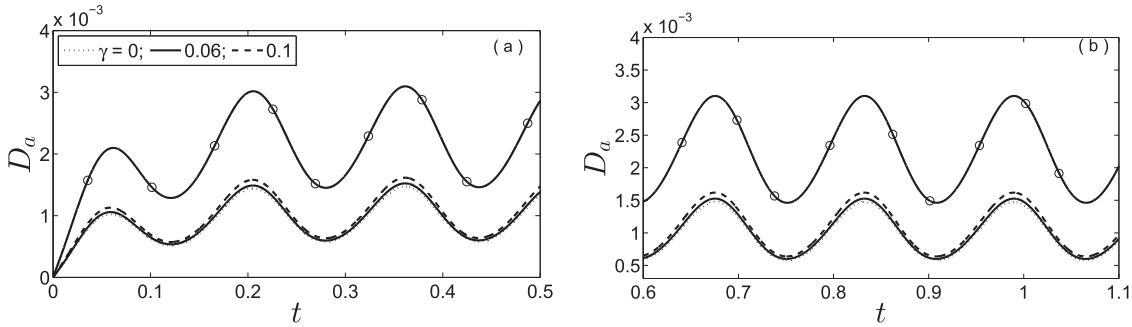

FIG. 17. Time assessment of dispersion coefficient D_a for various values of γ for the case $D_p = D_c = 1$, $\beta = 2$, $m = 1.4$, $n = 1.07$, $e = 0.3$, and $\alpha = 0.2$. When (i) $\tau_y = 0.04$, $\gamma = 0$, 0.06, 0.1 and (ii) $\tau_y = 0$, $\gamma = 0$ (circle line).

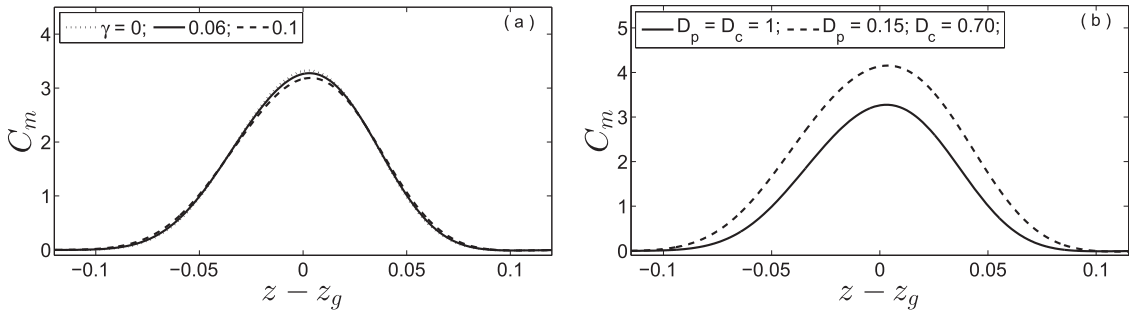

FIG. 18. Axial distribution of mean concentration for combined flows when $\tau_y = 0.04$, $\beta = 2$, $m = 1.4$, $n = 1.07$, $e = 0.3$, and $\alpha = 0.2$; (a) peripheral layer thickness when $D_p = D_c = 1$, and (b) diffusivity when $\gamma = 0.06$; at a fixed time, $t = 0.5$.

The molecular diffusivity or diffusion coefficient (D) is a kinematic property of the fluid which implies that the mass of the substance diffuses through a unit surface in a unit time at a concentration gradient of unity. So, diffusion coefficient (D) represents the spreading process, the larger value of D indicates the rapid spreading of the tracer curve whereas smaller D implies slow spreading of the solute in the liquid. Figure 16 shows the effect of various D on the apparent dispersion coefficient D_a. Figures are arranged in a manner that every first and second figures of each row in Fig. 16 show the observations for small and large time, respectively, under identical situation. On the way of expectation, Fig. 16 shows that larger values of diffusivity belonging to the region $\mathcal{R}_c$ or plug region $\mathcal{R}_p$ result in the decrease in the dispersion coefficient. The reason for this decrement is due to the fast spreading of molar flux. Also it can be easily observed from the figures that molecular diffusivities make strong influence on the dispersion process at the developed stage.

While observing the effect of peripheral layer variation on the dispersion coefficient, a discernible impact has been found in Fig. 17 for small as well as large time interval. Figures 17(a) and 17(b) depict that D_a increases as the value of the peripheral layer thickness γ increases. It is observed from the present study that, for a purely Casson liquid flow (when $\gamma = 0$ and $\tau_y = 0.04$), the magnitude of the dispersion coefficient is less than the layered liquid flow (when $\gamma = 0.1$ or 0.06 and $\tau_y = 0.04$). The physical explanation about such kind of behaviour is that the larger value of γ makes the border region for the Newtonian liquid; hence, the velocity of the liquid increases resulting the higher convection and diffusion rate. Hence, if the liquid is only Newtonian (when $\gamma = 0$ and $\tau_y = 0$), it has the higher value of dispersion coefficient than the Casson and three-layer liquids, which can be seen from the circle line in Fig. 17.

The axial distribution of mean concentration under the variation of peripheral layer thickness and molecular diffusivity has been observed through the profiles presented in Figs. 18(a) and 18(b). Figure 18(a) shows that smaller value of γ is the reason for higher peak length. As evident from Fig. 18(b), stronger diffusivity makes continuous spreading of the solute in the radial direction resulting in the decrease in the peak height of mean concentration.

In a blood or blood-like liquid flow analysis, two-fluid model is significant as compared to single phase fluid models for small arteries. The two-phase models of core of suspended erythrocytes and a cell-free layer surrounding the core is among the good agreement for microvescular blood flow studies.[19,43] The non-Newtonian Casson fluid model is much suitable to represent the effect of red blood cell aggregation[15] and the surrounding cell free layer (plasma layer) is represented by the Newtonian fluid.[40] Though red blood cells are essential to deliver oxygen to the tissue, abnormally high levels can have deadly consequences, which can be approximated by hematocrit percentage. An increase in hematocrit will decrease the thickness of the cell free layer which in other way increase the amount of red blood cells, as a result, blockage can occur in the blood vessels. This condition may cause microvascular disease,[48] which is a further consequence of a disorder in blood supply to heart muscles and interior of the brain.[2] It can be concluded from the above discussion that the solute dispersion under the present model and its physiological consequences are significant for microcirculation. Again, by the consideration of some parameter values, the two-fluid model can be reduced to single layer Newtonian and Casson fluid models and hence the relative conclusions can be drawn for those models that have applications in the catheterized artery for large vessels.

IX. CONCLUSION

The study is performed to investigate the transport processes in terms of dispersion coefficient in a layered-liquid flow through a tube having catalytic wall reaction. A three-layer liquid flow is considered where the center liquid is the Casson liquid and the Newtonian liquid is surrounding the central liquid. It is already discussed that this kind of model can be useful for the mathematical analysis of blood flow, in addition, as the pulse presents in the carrier flow, the study has significant implication. In contrast to existing literatures, the present work follows the effect of viscosity and density ratios in the solute transport process. As different molecular diffusivities are considered in different liquid layers, and peripheral layer effect is measured during transport of materials, the present model is more generalized and pronounced in this paradigm of the study. The following general conclusions can be made from the study.

(a) In the case of a steady flow and unsteady convective diffusion of reactive solute, dispersion coefficient is found to decrease with absorption parameter, yield stress, and viscosity ratio; however, it is independent of density ratio.

(b) In the case of a purely unsteady and combined flow, dispersion coefficient is decreased by absorption parameter, yield stress, and viscosity ratio. However a non-uniform behaviour of the dispersion coefficient has been observed for varying density ratio though it may increase the speed of the dispersion.

(c) The peripheral layer enhances the value of the dispersion coefficient and this result can be attributed to the large value of the layer depth in comparison with that of the Casson liquid.

(d) Stronger absorption results in a much flat trend of mean concentration distribution and also the peak of the mean concentration distribution rises when the yield stress and viscosity ratio increase, whereas peak of the distribution shows an inhomogeneous pattern with the increment of density ratio.

(e) As diffusivity increases, dispersion coefficient decreases, consequently peak of the mean concentration distribution also goes downward.

(f) Dispersion coefficient decreases with the increase in the value of yield stress.

(g) At the initial time, dispersion coefficient is less affected by absorption at the boundary though at the large time the effect is pronounced.

(h) Initially viscosity ratio reduces the magnitude of the dispersion coefficient but ultimately leads to a steady value.

(i) The findings of the study are significantly important for dispersion in blood-like liquid flow.

APPENDIX A: DERIVATION OF VELOCITY PROFILE IN THE THREE-LAYER REGION USING REGULAR PERTURBATION METHOD

The dimensionless momentum form of Eqs. (2)–(5) is

$$n\,\epsilon\frac{\partial u_c}{\partial t} = 4p(t) - \frac{1}{r}\frac{\partial(r\,\tau_c)}{\partial r} \quad 0 \le r \le R_o, \tag{A1}$$

$$\epsilon\frac{\partial u_n}{\partial t} = 4p(t) - \frac{1}{r}\frac{\partial(r\,\tau_n)}{\partial r} \quad R_o \le r \le 1, \tag{A2}$$

$$\left.\begin{array}{llll} \tau_c^{\frac{1}{2}} = \tau_y^{\frac{1}{2}} + (-m\,\frac{\partial u_c}{\partial r})^{\frac{1}{2}} & \text{if} \quad \tau_c \ge \tau_y & \text{for} & R_p \le r \le R_o \\ \frac{\partial u_c}{\partial r} = 0 & \text{if} \quad \tau_c \le \tau_y & \text{for} & 0 \le r \le R_p \\ \tau_n = -\frac{\partial u_n}{\partial r} & \text{if} \quad \tau_y = 0 & \text{for} & R_o \le r \le 1 \end{array}\right\}, \tag{A3}$$

$$\left.\begin{array}{ll} \tau_c \text{ is finite and } \frac{\partial u_c}{\partial r} = 0 & \text{at } r = 0, \\ \tau_c = \tau_n \text{ and } u_c = u_n & \text{at } r = R_o, \\ u_n = 0 & \text{at } r = 1, \end{array}\right\}. \tag{A4}$$

Here $p(t) = \left(1 + e\,\sin(\alpha^2\,Sc\,t)\right)$, $\epsilon = \frac{1}{Sc}$ is the inverse of the Schmidt number. m and n are the viscosity and density ratios.

To solve the boundary value problem for the time-periodic fluid flow, we consider a regular perturbation solution of the form considering ϵ is small,

$$\left.\begin{array}{l} u_c(r,t) = u_{0c}(r,t) + \epsilon\,u_{1c}(r,t) + \cdots, \\ u_n(r,t) = u_{0n}(r,t) + \epsilon\,u_{1n}(r,t) + \cdots, \\ \tau_c(r,t) = \tau_{0c}(r,t) + \epsilon\,\tau_{1c}(r,t) + \cdots, \\ \tau_n(r,t) = \tau_{0n}(r,t) + \epsilon\,\tau_{1n}(r,t) + \cdots. \end{array}\right\} \tag{A5}$$

Utilizing Eq. (A5) in Eqs. (A1)–(A4), we get

Zeroth order terms

$$\frac{\partial}{\partial r}(r\tau_{0c}) = 4p(t)r, \tag{A6}$$

$$-m\frac{\partial u_{0c}}{\partial r} = \tau_{0c} + \tau_y - 2\tau_y^{\frac{1}{2}}\tau_{0c}^{\frac{1}{2}}, \tag{A7}$$

$$\frac{\partial}{\partial r}(r\tau_{0n}) = 4p(t)r, \tag{A8}$$

$$\tau_{0n} = -\frac{\partial u_{0n}}{\partial r}. \tag{A9}$$

First order terms

$$n\frac{\partial u_{0c}}{\partial t} = -\frac{1}{r}\frac{\partial}{\partial r}(r\tau_{1c}), \tag{A10}$$

$$-m\frac{\partial u_{1c}}{\partial r} = \tau_{1c}\left(1 - \sqrt{\frac{\tau_y}{\tau_{0c}}}\right), \tag{A11}$$

$$\frac{\partial u_{0n}}{\partial t} = -\frac{1}{r}\frac{\partial}{\partial r}(r\tau_{1n}), \tag{A12}$$

$$\tau_{1n} = -\frac{\partial u_{1n}}{\partial r}. \tag{A13}$$

The boundary conditions for solving Eqs. (A6)–(A13) are

$$\left.\begin{array}{ll} \tau_{0c} \text{ and } \tau_{1c} \text{ are finite and } \frac{\partial u_{0c}}{\partial r} = 0, \frac{\partial u_{1c}}{\partial r} = 0 & \text{at } r = 0, \\ \tau_{0c} = \tau_{0n}, \tau_{1c} = \tau_{1n}, u_{0c} = u_{0n}, u_{1c} = u_{1n} & \text{at } r = R_o, \\ u_{0n} = u_{1n} = 0 & \text{at } r = 1, \end{array}\right\}. \tag{A14}$$

Solving the boundary value problem of Eqs. (A6)–(A14), we get

$$\tau_{0c} = 2p(t)\,r, \tag{A15}$$

$$u_{0c}(r,t) = \frac{p(t)}{m}\left[m(1-R_o^2) + R_o^2\left\{1 - \xi_1^2 - \frac{4\sqrt{2}}{3}\xi_2^{\frac{1}{2}}\left(1 - \xi_1^{\frac{3}{2}}\right) + \xi_2\,(1-\xi_1)\right\}\right], \quad R_p \le r \le R_o, \tag{A16}$$

$$\tau_{0n} = 2p(t)\, r, \tag{A17}$$

$$u_{0n}(r,t) = p(t)(1-r^2), \quad R_o \le r \le 1, \tag{A18}$$

$$\tau_{1c} = -\frac{n\, p'(t)}{m}\left[\frac{r\, m}{2}(1-R_o^2) + R_o^2\left\{\frac{r}{2} - \frac{r^3}{4R_o^2} - \frac{2\sqrt{2}}{3}\sqrt{\frac{\tau_y}{R_o\, p(t)}}\left(\frac{r}{2} - \frac{2}{7}\frac{r^{5/2}}{R_o^{3/2}}\right)\right\}\right], \tag{A19}$$

$$u_{1c}(r,t) = \frac{p'(t)}{16}\left[\frac{n}{m}R_o\ \log(R_o)\left\{8\, m\, R_o(1-R_o^2) + R_o^3\left(4 - \frac{16\sqrt{(2\xi_2)}}{7}\right)\right\} - R_o^4 + 4R_o^2 - 3 - 4R_o^2(2-R_o^2)\log(R_o) - \frac{4n}{m}R_o^2(1-R_o^2)(1-\xi_1^2) - \frac{n}{m^2}R_o^4\left\{3 - \frac{32\sqrt{2\xi_2}}{3}\left(\frac{33}{196} - \frac{\xi_1^2}{4} + \frac{4}{49}\xi_1^{\frac{7}{2}}\right) - 4\xi_1^2 + \xi_1^4\right\} + \frac{16}{3\sqrt{2}}\frac{n}{m}R_o^2(1-R_o^2)\left(1-\xi_1^{\frac{3}{2}}\right) + \frac{16R_o^4 n}{\sqrt{2}m^2}\sqrt{\xi_2}\left\{\frac{11}{42} - \frac{2\sqrt{2}}{3}\xi_2^{\frac{1}{2}}\left(\frac{5}{21} - \frac{1}{3}\xi_1^{\frac{3}{2}} + \frac{2}{21}\xi_1^3\right) - \frac{1}{3}\xi_1^{\frac{3}{2}} + \frac{1}{14}\xi_1^{\frac{7}{2}}\right\}\right], \quad R_P \le r \le R_o, \tag{A20}$$

$$\tau_{1n} = -p'(t)\left[\frac{r}{2} - \frac{r^3}{4} - \frac{R_o^2}{2r} + \frac{R_o^4}{4r} + \frac{nR_o}{mr}\left\{\frac{m}{2}R_o\ (1-R_o^2) + R_o^3\left(\frac{1}{4} - \frac{1}{7}\sqrt{\frac{2\tau_y}{p(t)R_o}}\right)\right\}\right], \tag{A21}$$

$$u_{1n}(r,t) = \frac{p'(t)}{16}\left[\frac{n}{m}\ R_o\ \log(r)\left\{8\, m\, R_o(1-R_o^2) + R_o^3\left(4 - \frac{16\sqrt{2\xi_2}}{7}\right)\right\} - r^4 + 4r^2 - 3 - 4R_o^2(2-R_o^2)\log(r)\right], \quad R_o \le r \le 1. \tag{A22}$$

The plug flow velocity counterparts u_{op} and u_{1p} can be obtained by taking $r = R_p$ in Eqs. (A16) and (A20)

$$u_{0p}(r,t) = \frac{p(t)}{m}\left[m(1-R_o^2) + R_o^2\left\{1 - \xi_2^2 - \frac{4\sqrt{2}}{3}\xi_2^{\frac{1}{2}} \times \left(1-\xi_2^{\frac{3}{2}}\right) + \xi_2(1-\xi_2)\right\}\right], 0 \le r \le R_p \tag{A23}$$

$$u_{1p}(r,t) = \frac{p'(t)}{16}\left[\frac{n}{m}R_o\ \log(R_o)\left\{8\, m\, R_o(1-R_o^2) + R_o^3 \times \left(4 - \frac{16\sqrt{(2\xi_2)}}{7}\right)\right\} - R_o^4 + 4R_o^2 - 3 - 4R_o^2 \times (2-R_o^2)\log(R_o) - \frac{4n}{m}R_o^2(1-R_o^2)(1-\xi_2^2) - \frac{n}{m^2}R_o^4\left\{3 - \frac{32\sqrt{2\xi_2}}{3}\left(\frac{33}{196} - \frac{\xi_2^2}{4} + \frac{4}{49}\xi_2^{\frac{7}{2}}\right) - 4\xi_2^2 + \xi_2^4\right\} + \frac{16}{3\sqrt{2}}\frac{n}{m}R_o^2(1-R_o^2)\left(1-\xi_2^{\frac{3}{2}}\right) + \frac{16R_o^4 n}{\sqrt{2}m^2}\sqrt{\xi_2}\left\{\frac{11}{42} - \frac{2\sqrt{2}}{3}\xi_2^{\frac{1}{2}}\left(\frac{5}{21} - \frac{1}{3}\xi_2^{\frac{3}{2}} + \frac{2}{21}\xi_2^3\right) - \frac{1}{3}\xi_2^{\frac{3}{2}} + \frac{1}{14}\xi_2^{\frac{7}{2}}\right\}\right], \quad 0 \le r \le R_p, \tag{A24}$$

where $\xi_1 = \frac{r}{R_o}$ and $\xi_2 = \frac{R_p}{R_o}$. Using the two-term perturbation series, we obtain the velocity distribution in the three layers in the form documented in Eqs. (17a)–(17c).

APPENDIX B: DERIVATION OF CENTRAL MOMENTS

Using the values p = 2, 3, and 4 in Eq. (24) gives

$$\mu_2(t) = \frac{\int_0^1\int_0^{2\pi}\int_{-\infty}^{+\infty} r(z-z_g)^2 C\mathrm{d}r\mathrm{d}\theta\mathrm{d}z}{\int_0^1\int_0^{2\pi}\int_{-\infty}^{+\infty} rC\mathrm{d}r\mathrm{d}\theta\mathrm{d}z}, \tag{B1}$$

$$\mu_3(t) = \frac{\int_0^1\int_0^{2\pi}\int_{-\infty}^{+\infty} r(z-z_g)^3 C\mathrm{d}r\mathrm{d}\theta\mathrm{d}z}{\int_0^1\int_0^{2\pi}\int_{-\infty}^{+\infty} rC\mathrm{d}r\mathrm{d}\theta\mathrm{d}z}, \tag{B2}$$

$$\mu_4(t) = \frac{\int_0^1\int_0^{2\pi}\int_{-\infty}^{+\infty} r(z-z_g)^4 C\mathrm{d}r\mathrm{d}\theta\mathrm{d}z}{\int_0^1\int_0^{2\pi}\int_{-\infty}^{+\infty} rC\mathrm{d}r\mathrm{d}\theta\mathrm{d}z}. \tag{B3}$$

Utilizing Eqs. (18) and (21) in Eqs. (B1)–(B3) gives

$$\mu_2(t) = \frac{\langle C^{(2)}\rangle - 2z_g\langle C^{(1)}\rangle + z_g^2\langle C^{(0)}\rangle}{\langle C^{(0)}\rangle}, \tag{B4}$$

$$\mu_3(t) = \frac{\langle C^{(3)}\rangle - 3z_g\langle C^{(2)}\rangle + 3z_g^2\langle C^{(1)}\rangle - z_g^3\langle C^{(0)}\rangle}{\langle C^{(0)}\rangle}, \tag{B5}$$

$$\mu_4(t) = \frac{\langle C^{(4)}\rangle - 4z_g\langle C^{(3)}\rangle + 6z_g^3\langle C^{(2)}\rangle - 4z_g^3\langle C^{(1)}\rangle + z_g^4\langle C^{(0)}\rangle}{\langle C^{(0)}\rangle}. \tag{B6}$$

Since

$$z_g = \frac{\int\int\int zC\mathrm{d}v}{\int\int\int C\mathrm{d}v} = \frac{\langle C^{(1)}\rangle}{\langle C^{(0)}\rangle},$$

the above Eqs. (B4)–(B6) reduce to Eq. (25) of central moments about mean.

[1] Agrawal, S. and Jayaraman, G., "Numerical simulation of dispersion in the flow of power law fluids in curved tubes," Appl. Math. Modell. **18**, 504 (1994).
[2] Ahmed, B., "New insights into the pathophysiology, classification, and diagnosis of coronary microvascular dysfunction," Coron. Artery Dis. **25**, 439 (2014).
[3] Ananthakrishnan, V., Gill, W. N., and Barduhn, A. J., "Laminar dispersion in capillaries: Part I. Mathematical analysis," AIChE J. **11**, 1063 (1965).
[4] Anderson, D., Tannehill, J. C., and Pletcher, R. H., *Computational Fluid Mechanics and Heat Transfer* (Hemisphere Publishing Corporation, New York, 1984).
[5] Aris, R., "On the dispersion of a solute in a fluid flowing through a tube," Proc. R. Soc. London, Ser. A **235**, 67 (1956).
[6] Aroesty, J. and Gross, J. F., "The mathematics of pulsatile flow in small vessels I. Casson theory," Microvasc. Res. **4**, 1 (1972).
[7] Bandyopadhyay, S. and Mazumder, B. S., "Unsteady convective diffusion in a pulsatile flow through a channel," Acta Mech. **134**, 1 (1999).
[8] Barton, N. G., "On the method of moments for solute dispersion," J. Fluid Mech. **126**, 205 (1983).
[9] Bayareh, M. and Mortazavi, S., "Effect of density ratio on the hydrodynamic interaction between two drops in simple shear flow," Iran. J. Sci. Technol., Trans. Mech. Eng. **35**, 121 (2011).
[10] Blair, G. W. S., "An equation for the flow of blood, plasma and serum through glass capillaries," Nature **183**, 613 (1959).
[11] Bugliarello, G. and Sevilla, J., "Velocity distribution and other characteristics of steady and pulsatile blood flow in fine glass tubes," Biorheology **7**, 85 (1970).
[12] Caro, C., Pedley, T. J., Schroter, R. C., and Seed, W. A., *The Mechanics of the Circulation* (Oxford University Press, 1978).
[13] Charm, S. and Kurland, G., "Viscometry of human blood for shear rates of 0-100,000 sec^{-1}," Nature **206**, 617 (1965).
[14] Cokelet, G. R., "The rheology of human blood," Biomech. Found. Obj. **72**, 63 (1972).
[15] Das, B., Johnson, P. C., and Popel, A. S., "Computational fluid dynamic studies of leukocyte adhesion effects on non-Newtonian blood flow through microvessels," Biorheology **37**, 239 (2000).
[16] Dash, R. K., Jayaraman, G., and Mehta, K. N., "Estimation of increased flow resistance in a narrow catheterized artery—a theoretical model," J. Biomech. **29**, 917 (1996).
[17] Dash, R. K., Jayaraman, G., and Mehta, K. N., "Shear augmented dispersion of a solute in a Casson fluid flowing in a conduit," Ann. Biomed. Eng. **28**, 373 (2000).
[18] Debnath, S., Saha, A. K., Mazumder, B. S., and Roy, A. K., "Hydrodynamic dispersion of reactive solute in a Hagen–Poiseuille flow of a layered liquid," Chin. J. Chem. Eng. **25**, 862 (2017).
[19] Fung, Y.-C., *Biomechanics* (Springer, 1993).
[20] Gill, W. N. and Sankarasubramanian, R., "Exact analysis of unsteady convective diffusion," Proc. R. Soc. A **316**, 341 (1970).
[21] Kim, C. and Bernal, L. P., AIAA Paper 2000-0855, 2000.
[22] Krishnan, B. C., Rittgers, S. E., and Yoganathan, A. P., *Biofluid Mechanics: The Human Circulation* (Taylor and Francis, USA, 2012).
[23] Marušić-Paloka, E. and Pažanin, I., "On reactive solute transport through a curved pipe," Appl. Math. Lett. **24**, 878 (2011).
[24] Mazumder, B. S. and Bandyopadhyay, S., "On solute dispersion from an elevated line source in an open-channel flow," J. Eng. Math. **40**, 197 (2001).
[25] Mazumder, B. S. and Das, S. K., "Effect of boundary reaction on solute dispersion in pulsatile flow through a tube," J. Fluid Mech. **239**, 523 (1992).
[26] Mazumder, B. S. and Mondal, K. K., "On solute transport in oscillatory flow through an annular pipe with a reactive wall and its application to a catheterized artery," Q. J. Mech. Appl. Math. **58**, 349 (2005).
[27] Mazumder, B. S. and Paul, S., "Dispersion of reactive species with reversible and irreversible wall reactions," Heat Mass Transfer **48**, 933 (2012).
[28] McDonald, D. A., *Blood Flow in Arteries* (Edward Arnold, London, 1974).
[29] Medvedev, A. E. and Fomin, V. M., "Two-phase blood-flow model in large and small vessels," Dokl. Phys. **56**, 610 (2011).
[30] Mehta, R. V., Merson, R. L., and McCoy, B. J., "Hermite polynomial representation of chromatography elution curves," J. Chromatogr. A **88**, 1 (1974).
[31] Nagarani, P., Sarojamma, G., and Jayaraman, G., "Exact analysis of unsteady convective diffusion in Casson fluid flow in an annulus—Application to catheterized artery," Acta Mech. **187**, 189 (2006).
[32] Nagarani, P. and Sebastian, B. T., "Dispersion of a solute in pulsatile non-Newtonian fluid flow through a tube," Acta Mech. **224**, 571 (2013).
[33] Ng, C.-O. and Rudraiah, N., "Convective diffusion in steady flow through a tube with a retentive and absorptive wall," Phys. Fluids **20**, 073604 (2008).
[34] Purtell, L. P., "Molecular diffusion in oscillating laminar flow in a pipe," Phys. Fluids **24**, 789 (1981).
[35] Rana, J. and Murthy, P. V. S. N., "Solute dispersion in pulsatile Casson fluid flow in a tube with wall absorption," J. Fluid Mech. **793**, 877 (2016).
[36] Rana, J. and Murthy, P. V. S. N., "Unsteady solute dispersion in Herschel-Bulkley fluid in a tube with wall absorption," Phys. Fluids **28**, 111903 (2016).
[37] Rana, J. and Murthy, P. V. S. N., "Unsteady solute dispersion in non-Newtonian fluid flow in a tube with wall absorption," Proc. R. Soc. A **472**, 20160294 (2016).
[38] Rana, J. and Murthy, P. V. S. N., "Unsteady solute dispersion in small blood vessels using a two-phase Casson model," Proc. R. Soc. A **473**, 20170427 (2017).
[39] Redapangu, P. R., Chandra Sahu, K., and Vanka, S. P., "A study of pressure-driven displacement flow of two immiscible liquids using a multiphase lattice Boltzmann approach," Phys. Fluids **24**, 102110 (2012).
[40] Sankar, D. S., "A two-fluid model for pulsatile flow in catheterized blood vessels," Int. J. Non-Linear Mech. **44**, 337 (2009).
[41] Sankar, D. S. and Lee, U., "Two-fluid Casson model for pulsatile blood flow through stenosed arteries: A theoretical model," Commun. Nonlinear Sci. Numer. Simul. **15**, 2086 (2010).
[42] Sarkar, A. and Jayaraman, G., "The effect of wall absorption on dispersion in oscillatory flow in an annulus: application to a catheterized artery," Acta Mech. **172**, 151 (2004).
[43] Sharan, M. and Popel, A. S., "A two-phase model for flow of blood in narrow tubes with increased effective viscosity near the wall," Biorheology **38**, 415 (2001).
[44] Sharp, M. K., "Shear-augmented dispersion in non-Newtonian fluids," Ann. Biomed. Eng. **21**, 407 (1993).
[45] Shaul, S. and Kalman, H., "Three plugs model," Powder Technol. **283**, 579 (2015).
[46] Siddheshwar, P. G., Markande, S., and Manjunath, S., "Effect of interphase mass transfer on unsteady convective diffusion: Part I, plane-Poiseuille flow of a power-law fluid in a channel," Chem. Eng. Commun. **180**, 187 (2000).
[47] Taylor, G., "Dispersion of soluble matter in solvent flowing slowly through a tube," Proc. R. Soc. London, Ser. A **219**, 186 (1953).
[48] Vahidkhah, K., Balogh, P., and Bagchi, P., "Flow of red blood cells in stenosed microvessels," Sci. Rep. **6**, 28194 (2016).